NICOLÁS IGNACIO ARAYA RIVERA

INFLUENCE OF HEAT TREATMENTS ON THE MICROSTRUCTURAL EVOLUTION AND MECHANICAL PROPERTIES OF SELF-LUBRICATING SINTERED STEEL

Dissertação de Mestrado apresentada ao Programa de Pós-Graduação em Ciência e Engenharia de Materiais, como requisito parcial para a obtenção do grau de Mestre em Ciência e Engenharia de Materiais.

Orientador: Aloisio Nelmo Klein
Co orientador: Claudio Aguilar

FLORIANÓPOLIS
2016

Ficha de identificação da obra elaborada pelo autor,
através do Programa de Geração Automática da Biblioteca Universitária da UFSC.

RIVERA, NICOLÁS ARAYA
INFLUENCE OF HEAT TREATMENTS ON THE MICROSTRUCTURAL EVOLUTION AND MECHANICAL PROPERTIES OF SELF-LUBRICATING SINTERED STEEL / NICOLÁS ARAYA RIVERA ; orientador, Aloisio Nelmo Klein ; coorientador, Claudio Aguilar. - Florianópolis, SC, 2016.
90 p.

Dissertação (mestrado) - Universidade Federal de Santa Catarina, Centro Tecnológico. Programa de Pós-Graduação em Ciência e Engenharia de Materiais.

Inclui referências

1. Ciência e Engenharia de Materiais. 2. tratamentos térmicos. 3. sinterização. 4. materiais autolubrificantes. I. Klein, Aloisio Nelmo. II. Aguilar, Claudio. III. Universidade Federal de Santa Catarina. Programa de Pós Graduação em Ciência e Engenharia de Materiais. IV. Título.

NICOLÁS ARAYA RIVERA

INFLUENCE OF HEAT TREATMENTS ON THE MICROSTRUCTURAL EVOLUTION AND MECHANICAL PROPERTIES OF SELF-LUBRICATING SINTERED STEEL

Esta Dissertação foi julgada adequada para obtenção do Título de "Mestre em Ciência e Engenharia de Materiais" e aprovada em sua forma final pelo Programa de Pós-Graduação em Ciência e Engenharia de Materiais.

Florianópolis, 26 de Fevereiro de 2016.

_____
Prof. Dr. Antônio Pedro Novaes de Oliveira
Coordenador do Curso

_____	_____
Prof. Dr. Ing. Aloísio Nelmo Klein Orientador	Prof. Dr. Ing. Claudio Aguilar Ramirez Coorientador

Banca Examinadora:

_____	_____
Prof. Dr. Ing. Cesar Edil da Costa UDESC/Joinville	Prof. Dr. Eng. Jose Daniel Biasoli de Mello Universidade Federal de Uberlândia

_____
Dr. Eng. Tatiana Bendo
Universidade Federal de Santa Catarina

To my daugther who will have an entire world to explore and learn as long she never stop pursuing her dreams.

AGRADECIMENTOS

Ao Professor Dr. Claudio Aguilar por me motivar para fazer a minha pós-graduação numa instituição de excelência e também pela paciência ao longo do processo.

Ao Professor Dr. Aloisio Nelmo Klein pela maravilhosa acolhida e apoio desde a minha primeira visita no LabMat no ano 2012.

Ao Dr. Cristiano Binder pela orientação na parte teórica e prática e pela excelente disposição na hora de resolver qualquer dúvida ou problema.

A minha namorada Paula Aranda pela paciência e apoio durante esta fase

Ao Rogério Antônio Campos pela eficiência com a qual desempenha seu trabalho frente a secretaria do PGMAT/UFSC. Pela simpatia e disposição em sempre auxiliar os alunos.

Aos companheiros do LabMat pelo bom convívio, motivação e ajuda dispensada durante este período. Especialmente aos meus colegas de sala Caroline, Luiz, Gilberto, Nilda, Maisa e Cleber pela acolhida, os risos e pelo auxílio na hora de me adaptar na vida Brasileira.

Ao BNDES e ao CNPQ e CAPES pelo financiamento da pesquisa.

E a todos aqueles que contribuíram, de maneira direta ou indireta, para o êxito na conclusão do mestrado.

"Where there is a tree to be planted, you plant it. Where there is an error to be corrected, correct it. There is always an effort that everybody dodges, you do it. You be the one that moves the rock away of the road"

Gabriela Mistral

"I'm of those who think that science has a great beauty. A scientist in his laboratory is not a mere technician: he is also a child confronting natural phenomena that impress him as though they were fairy tales"

Marie Curie

RESUMO

A pesquisa e desenvolvimento de materiais autolubrificantes estão diretamente associados com o desejo de diminuir o consumo de energia em aplicações onde lubrificantes fluidos são indesejados. Pesquisar e caracterizar as suas propriedades se torna crítico quando as aplicações requerem uma resistência mecânica maior da que os materiais atualmente disponíveis. O escopo do presente trabalho é caracterizar as propriedades mecânicas e o comportamento da microestrutura de aços sinterizados autolubrificantes com adições de SiC o que atua como precursor na formação de nódulos de grafita dentro do material. Este processo foi previamente desenvolvido pelo equipe de pesquisa do LabMat/UFSC.

A liga utilizada como matriz foi Fe + 0.45C + 4Ni + 1Mo % em massa com adições de 2 e 3% de SiC. A rota de processamento foi: Moldagem de Pós por Injeção, seguido de remoção química de ligantes e remoção de ligantes e sinterização assistida por plasma (PADS pelas suas siglas em inglês) seguido de martempera a 180 °C, duas condições de revenido (530 e 300 °C) e austempera a 300 °C para gerar 4 condições para cada liga estudada.

A temperabilidade e os parâmetros para os tratamentos térmicos foram determinados utilizando dilatometria diferencial e simulações por software. A dureza, as tensões de escoamento e máxima assim como a capacidade de endurecimento por deformação foram estudadas utilizando medições de dureza e ensaios de tensão uniaxial. A microestrutura foi analisada por microscopia ótica, microscopia eletrônica de varredura, espectroscopia de energia dispersiva e medições de micro dureza. Os resultados do presente trabalho mostram que a dissolução parcial do Ni na liga matriz afeta a microestrutura e o comportamento ao longo do tratamento térmico junto com o Mo, por outra parte o Si dissolvido na matriz produto da dissociação do SiC afeta notoriamente a morfologia da microestrutura e o comportamento dilatométrico do material sob condições de aquecimento e resfriamento.

Palavras-chave: tratamentos térmicos, sinterização, materiais autolubrificantes.

X

ABSTRACT

Self-lubricating materials research and development are directly linked with the pursuing of energy savings in applications were fluid lubricants are undesired. Researching and characterizing its properties becomes critical when the applications require higher mechanical resistance than of the materials currently available. The scope of this work is to characterize the mechanical and microstructural behavior of sintered self-lubricating steels with SiC additions acting as a precursor phase for graphite nodules, this process route was previously developed by the research team of LabMat/UFSC.

The alloy used as matrix was Fe + 0.45C + 4Ni + 1Mo wt% with additions of 2 and 3 wt% SiC. The process route was: Metal Injection Molding, then chemical debinding and Plasma Assisted Debinding and Sintering (PADS) followed by 3 different heat treatments: martempering at 180 °C and tempering at 530 °C and 300 °C respectively and austempering at 300 °C to generate 4 different conditions for each studied alloy

Hardenability and heat treatments parameters were determined using dilatometric tests and software simulations. Hardness, yield and tensile strength and strain hardening behavior were studied using hardness measures and uniaxial mechanical testing. The microstructure was analyzed by optical microscopy, scanning electron microscopy, energy dispersive spectroscopy and microhardness indentations. The findings of this work shows that partial dissolution of Ni in the matrix affects both microstructure and behavior during heat treatments as well as Mo, on the other hand dissolved Si in the matrix due SiC dissolution notably affects the morphology of the microstructure and the material dilatometric behavior under heating and cooling conditions

Key-words: heat treatment, sintering, self- lubricating materials.

LIST OF FIGURES

LIST OF TABLES

LIST OF ABREVIATURES AND ACRONYMS

ABNT – Associação Brasileira de Normas Técnicas
IBGE – Instituto Brasileiro de Geografia e Estatístic
A1 – Lower austenitic transformation temperature
A3 – Upper austenitic transformation temperature
BS – Bainitic transformation start
BF – Bainitic transformation finish
CCT – Continuous Cooling Transformation
EDS – Energy Dispersive Spectroscopy
LABMAT – Laboratorio de Materiais
MS – Martensitic transformation start temperature
PIM – Powder Injection Molding
PS – Pearlitic transformation start
PF – Pearlitic transformation finish
SEM – Scanning Electron Microscope
SiC – Silicon Carbide
UFSC – Universidade Federal de Santa Catarina
UTS – Ultimate Tensile Strenght
YS – Yield Strenght

INDEX

1. INTRODUCTION

The growing development of society and technology is closely related to the research of new and better materials. In this context the energetic efficiency and the mechanical behavior of machines and its components have been one of the most relevant focuses of research to the industry in the last years, hence, new materials capable of decreasing energy loses by friction and at the same time, suitable for severe mechanical and tribological conditions have been developed

In conditions where the friction coefficient can't be decreased by using liquid lubricants (for example, high vacuum or high temperature conditions), solid lubrication appears as an alternative to conventional lubrication by creating a solid layer that prevents the direct contact between surfaces in relative movement. Usually solid lubricants shows a low shear strength and low molecular compression which allows the formation and maintenance of the required lubricating layer (STACHOWIAK; BATCHELOR, 2006)

One of the research lines of the 'Laboratorio de Materiais' of the Universidade Federal de Santa Catarina (LABMAT/UFSC) is the developing and characterization of dry self-lubricating steels produced by powder metallurgy. These steels have the property that the microstructural component which provides the solid lubrication is produced "in situ" during the sintering step. The in situ generation of the lubricating phase prevents the formation of a lubricant layer between the powder particles when de lubricating phase is added into the mixture of powders, previous to the sintering step. This lubricating layer hinders the sintering process and makes impossible to attain the desired mechanical properties. The precursor for the in situ formation of the lubricating phase in the steels developed by the LABMAT is silicon carbide (SiC) which, during sintering, dissociates as $C_{graphite}$ + Si in solid solution (DE MELLO et al., 2013)

Currently the mechanical and tribological behavior of low alloy steels with SiC contents of 1,2,3,4 and 5% (BINDER, 2009) and the morphology and growth kinetics of graphite nodules (REBELO, 2014) have been studied. These previous research shows that the addition of Ni in the ferrous matrix produces a lower friction coefficient in these steels being this effect reinforced by the addition of Mo by hardening the matrix and affecting the shape of the graphite nodules, both

elements, besides producing a decrease in the friction coefficient, considerably increases the hardenability of these new alloys. Besides the previous studies, there are many challenges and opportunities in this field, such as improving mechanical and tribological properties through a better understanding of how both the lubricating phase and the matrix phases forms and interacts when sliding onto another surface. As heat treatment can severely affect the properties of ferrous alloys, the objective of this work is to characterize the influence of heat treatment in the microstructure and mechanical properties of SiC based self-lubricating sintered steels.

2. OBJECTIVES AND MOTIVATION

The current work has as objective to generate and characterize various self-lubricating steels produced by Powder Injection Molding (PIM) with a common ferrous matrix and variable SiC contents. This work is part of one of LABMAT research lines consisting in the development of new self-lubricating materials.

2.1 OVERALL OBJECTIVE

To study the relationship between mechanical properties and the microstructure obtained by cooling inside the reactor, austempering at 300 °C and martempering + tempering at two different temperatures (300 °C and 530 °C) of self-lubricating steel alloys obtained by Metal Injection Molding. The alloy to be used will consist in a ferrous matrix with 0.45% C, 4% Ni, and 1% Mo in weight with SiC contents of 0, 2 and 3 wt%.

2.2 SPECIFIC OBJECTIVES

- To study the effect of heat treatments in the microstructures obtained
- To evaluate the effect of the obtained microstructures of the ferrous matrix in the mechanical properties of the self-lubricating alloys
- To study the influence of SiC content in the properties of the heat treated steels.

3. LITERATURE REVIEW

3.1 SOLID LUBRICATION

Friction and wear are caused by contact and relative movement between two surfaces. A method to reduce both is to place a lubricating layer that can be a solid, oil, grease or gas. Machinery elements such as bearings, rails, cylinders, flexible couplings, chains and others possess surfaces that move relatively to each other by sliding, rolling, approaching and moving away of each other or combinations of these movements, therefore, these components are lubricated to prevent or decrease the contact between the surfaces. Mobile parts are lubricated by placing and maintaining films that minimize the contact between the surfaces and that are easily sheared and as a consequence: the friction force that goes against the movement of such surfaces is lowered. If direct contact between the surfaces occurs the friction forces involved are drastically risen which results in high temperatures and wear (MIYOSHI, 2001)

Without lubrication most of the machinery would have its lifespan greatly reduced. With inadequate lubrication the excessive wear would be the most severe consequence, because the point in which the machinery components can no longer be used will be quickly achieved and therefore the components will have to be retired from service and repaired accordingly. Reparations costs might be high, but productivity losses can surely be the most expensive consequences. With insufficient lubrication even if the components haven't failed the friction forces between the surfaces are so elevated that the engines might be overloaded thus generating excessive energy losses (MIYOSHI, 2001)

A solid lubricant is any material applied as a fine layer or powder into a surface to reduce friction and wear. Solid lubrication is obtained by using self-lubricating materials or a third solid body of low friction coefficient between the moving surfaces (CLAUSS, 1972). Oils and greases have a wide application range where they can be used successfully, however, they may present difficulties in their application such as sealing issues, excessive load or under extreme environmental conditions. Solid lubricants will be rather preferred over liquid or gaseous lubricants for several reasons: in high vacuum applications, spatial equipment or in the food industry the liquid lubricants could be

evaporated, polluting products such as food, optical and electronical equipment. At high temperatures the liquid lubricants are decomposed and oxidized and at cryogenic temperatures the liquid lubricants are highly viscous becoming unsuitable for lubrication (MIYOSHI, 2001).

Table 1 shows some applications where fluid lubrication is undesirable.

Table 1 - Applications where fluid lubricants are undesirable or unsuited.

Requirement	Application
To avoid contamination of the product or the environment	Food processing
	Space telescopes
	Microscopes and cameras
	Paper processing
	Medical equipment
To provide and maintain lubrication in hard to reach areas	Planes
	Space vehicles
	Satellites
	Nuclear reactors
Abrasion resistance in dirty environments	Space rovers
	Cars
	Mining equipment
	Off-road vehicles
	Construction equipment
To provide stationary service	Planes
	Train engines
	Missile components
	Telescope frames
	Furnaces

Source: Adapted by the author from MIYOSHI (2001)

Currently several different methods have been developed for the application of solid lubrication, for example, it can be provided by deposited DLC layers (ÖZMEN; TANAKA; SUMIYA, 2000; ZHANG; SHEN; SUN, 2010), BCN (DENG et al., 2014), polymer based composite layers (ZOUARI et al., 2014), etc. Solid lubrication can be also provided by incorporating solid lubricant in the bulk material by powder pressing (KATO et al., 2003; KOVÁČIK et al., 2008) or metal injection molding (MIM) (FURLAN et al., 2012). The solid lubricant can be also be generated in-situ using MIM which, besides incorporating the desired precursor in the bulk material, allows the microstructural design appropriated for in situ generation of the lubricating phase (SCHROEDER et al., 2010).

3.2 METAL INJECTION MOLDING

Powder metallurgy technologies have had a great development in the recent decades resulting into a very interesting technique for engineers, not only for its reproducing capabilities, but also because it allows to its users to plan the microstructure of the molded pieces by selectively adding phases or pores, adapting the product for its application. Powder metallurgy techniques enables the production of solid bodies, similarly to casting processes, but while casting processes only are technically/economically feasible for low to mid melting point metals, powder metallurgy can be applied to almost all of them (ASM INTERNATIONAL HANDBOOK COMMITEE, 1998). Thereby most of the available products made by powder metallurgy aren´t available as cast materials for example: composites, high temperature ceramics, some polymers, refractory metals and a wide variety of intermetallic compounds, cermets and mixed materials. For industrial production costs are always a critical factor, so the possibility of producing complex shapes in its final form has an important economic benefit, in powder technologies this relies on the capability to replicate the mold over and over again (GERMAN, 2005).

Products produced by injection molding have a wide range of uses, mainly for its low costs and high complexity of shapes (GERMAN, 2005). Metal injection molding use that principles by using a feed with a high content of thermoplastic particles. The steps of this process are shown in Fig. 1.

Fig. 1 - Powder Injection Molding process route

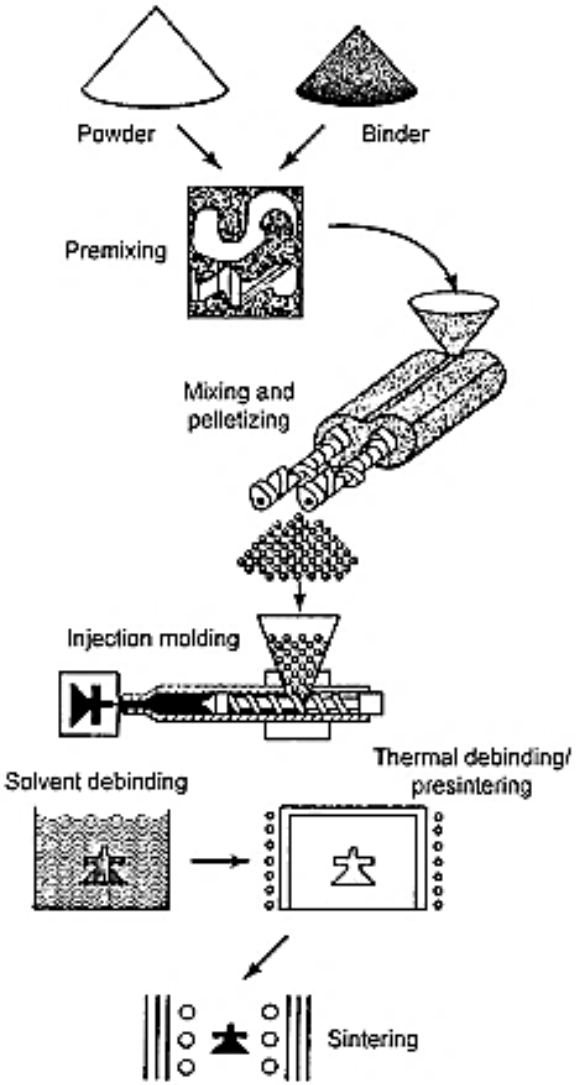

Source: ASM INTERNATIONAL HANDBOOK COMMITTEE (1998)

The process begins with the mixture of the selected powders and binders. Particles of powders used in this process often have average sizes below 20 μm with near spherical shapes. Binders are thermoplastic

mixes of waxes, polymers, oils, lubricants and surfactants. The binder imparts viscous flow properties to the mixture allowing it to fill mold with complexes geometries. When the binder freezes in the die, the piece is ejected. Finally the binder is removed and the powder structure is sintered. The product may then be further densified, heat threated or machined.

The equipment used for shaping is similar to what is used in plastic injection. Fig. 2 shows a cross-section of a MIM unit. Most molding machines fill a die through a gate from a pressurized and heated barrel. A plunger or a reciprocating screw generates the pressure needed to fill the die. Fig. 3 provides a conceptual outline of the molding sequence (GERMAN, 2005).

Fig. 2 - Cross-sectional sketch of the operating region of an injection machine

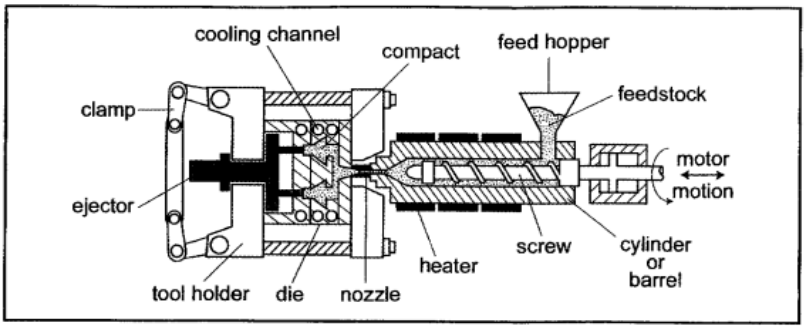

Source: RANDALL GERMAN (2005)

Fig. 3 - Sketch of the operation of the injection machine through one cycle

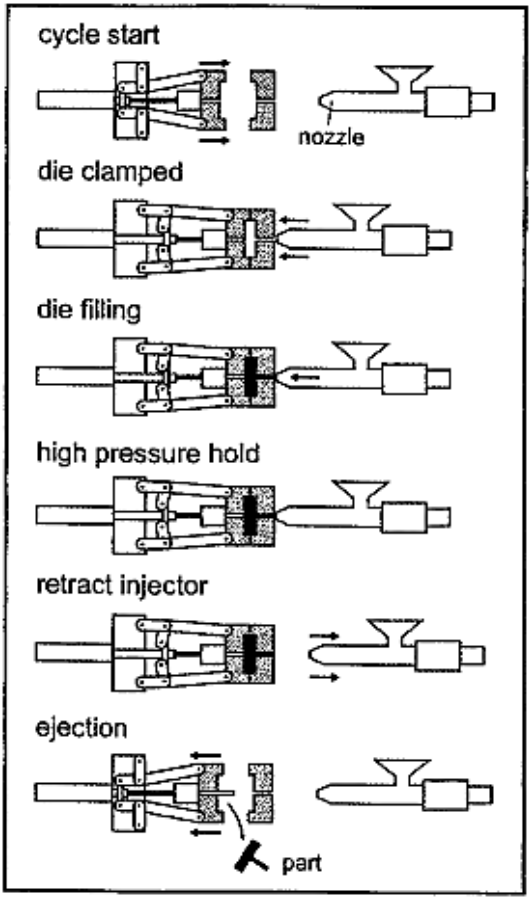

Source: RANDALL GERMAN (2005)

The metal injection molding process is practiced with many variations, yet the basic principles are similar: small polymeric particles are used to aid in the densification during sintering, this particles are referred as the binding system. The binding system is formulated to attain a high packing density with a low viscosity, is also required for it to have enough lubricant to fill the inter-particular gaps and to lubricate the sliding between particles in the molding process (GERMAN, 2005). The binder is mainly composed by two or three components, for example, 65% paraffin wax, 30% polypropylene and 5% stearic acid for

a 6% in mass for steel injection. In this work the binder is composed by a mixture of thermoplastic resin, plasticizer, lubricant, surfactant and anti-oxidant being an 8% of the feed total mass, this is required to obtain the required characteristic for the materials studied in this work: the self-lubricating steels.

3.3 SELF-LUBRICATING STEELS

Dry self-lubricating components have been used for decades in domestic and desktop equipment such as printers, electric shavers and blenders. Metallic matrixes of these components are commonly made of cooper, iron and nickel. Compounds such as MoS2, WS2, low melting point metals as silver, tin and lead and also graphite are the most used as solid lubricants (CUI et al., 2013; DU et al., 2012; FURLAN et al., 2012; KATO et al., 2003; MOUSTAFA et al., 2002). A great share of the self-lubricating composites developed in the past have a high percent of solid lubricant (15 to 40% v/v). This is added to obtain the required friction coefficient, however has as a consequence a discontinuous metallic matrix, hence, low mechanical properties (BINDER et al., 2010).

In the case of the sintered self-lubricating steels developed by the Laboratorio de Materiais from the Universidade Federal de Santa Catarina (LabMat/UFSC), the lubricating particles (graphite) are generated in-situ during the sintering process. In this case the ideal precursor particle is those which is composed by an element that has both a high solubility into iron and a strong ferrite stabilizing behavior and an element that form a lubricating phase when the precursor is decomposed yet don't solubilizes into the iron matrix, this is why the self-lubricating steels developed in the LabMat uses silicon carbide (SiC) particles as precursor phase.

The dispersed solid lubricant must form a completely discontinuous phase, for example, discrete particles uniformly distributed in the base metal. Big lubricating particles will form a discontinuous phase, however they will be prejudicial to the mechanical properties, small particles may form a continuous phase which will also be prejudicial to the mechanical properties, therefore exist an optimal size for the dispersed lubricating particles and thereby exist a free mean path between them which allows the metallic matrix to be completely continuous (BINDER et al., 2010). Fig. 4 presents an example of the

desired situation. In theory a regular distribution of solid lubricant particles means that each particle has to provide enough lubricant for a well-defined surface area.

Fig. 4 - Ideal distribution of lubricating particles in a sintered material

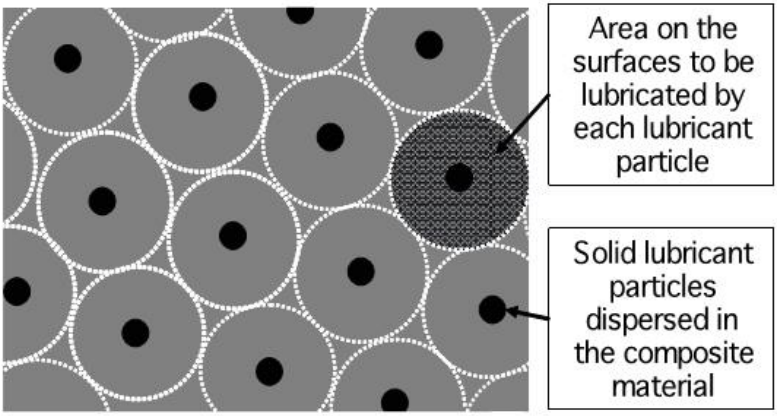

Source: Binder (2009)

The study of the dissociation of SiC in a steel matrix was done by both (BINDER, 2009) and (REBELO, 2014). The latter particularly studied the SiC content influence in the structure of the graphite generated during sintering and the influence of alloy elements, particularly Ni in SiC dissociation kinetics and Si-C dissolution into the ferrous matrix. The influence of the alloys elements in graphite morphology was also studied.

A strong dependence between time-temperature, SiC dissolution and microstructural evolution was found. For samples sintered below 1050 °C, SiC dissociation isn't complete showing larger graphite nodules in the gap between 1100 °C up to 1200 °C. It was also found that for short sintering times SiC dissociation isn't complete and for longer sintering times (more than 120 minutes at 1100 °C) completely homogenization occurs and the graphite nodules are completely dissolved (BINDER, 2009).

The graphite generated by SiC dissociation is turbostratic (BINDER, 2009; REBELO, 2014). Turbostratic graphite is a carbon allotrope with a sp2 hybridation state which presents a parallel random stacking with no tridimensional order. Volume properties are essentially

isotropic. In turbostratic graphite the net spacing (c axis) is ≥ 0.34 nm, exceeding those of crystalline graphite which is of 0.334 nm (DRESSELHAUS, 1997; REBELO, 2014; WELZ, 2003). The turbostratic stacking can be found mainly in carbon materials obtained at low temperatures, where the hexagonal layers are usually small and few of them are parallel stacked. Turbostratic graphite is produced mainly due to lattice defects such as stacking faults, vacancies and dislocations (WELZ, 2003).

Figs. 5 and 6 shows the difference between crystalline graphite and turbostratic graphite stacking.

Fig. 5 - Difference between crystalline (a) and turbostratic (b) graphite stacking

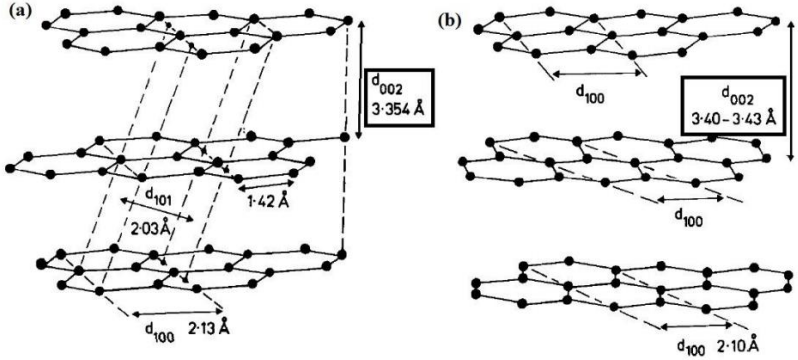

Source: Knox et al. (1986)

Fig. 6 - Upper view of graphite layers for crystalline stacking (a) and turbostratic stacking (b)

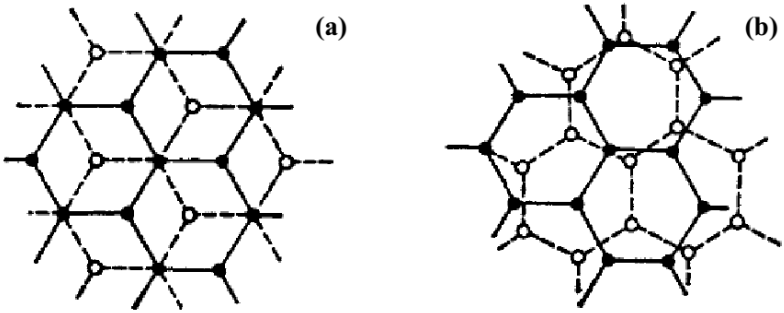

Source: Rebelo (2014)

It can be noticed that crystalline graphite shows a regular array of graphite layers stacked in order to minimize the spacing between layers meanwhile turbostratic graphite have a random stacking order in the c axis.

On the other hand mechanical and tribological properties of these steels were studied in (BINDER, 2009). The objective of the mentioned study therefore was to produce PIM sintered steels with variable contents of SiC, Ni and Mo. The Fe powder used was the BASF CL-OM produced by the carbonyl process with carbon and oxygen contents of 0.8 and 0.2 wt% respectively and to study its mechanical and tribological properties. The fig. 7 particularly shows the variation of the scuffing resistance and friction coefficient with SiC content on a Fe + 0.6C steel matrix, the fig 8 shows the variation of mechanical properties with SiC content on the same steel matrix, the samples where sintered at 1150 °C and then cooled inside the reactor, no further heat treatments where performed.

Fig. 7 - Relationship between scuffing resistance and friction coefficient with SiC content in a Fe + 0.6C self-lubricating PIM sintered steel

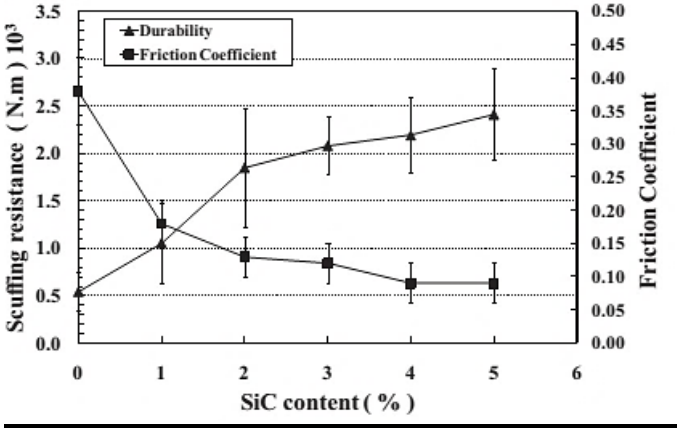

Source: De Mello et al. (2011)

Fig. 8 - Relationship between mechanical properties and SiC content of a Fe + 0.6C self-lubricating PIM sintered steel

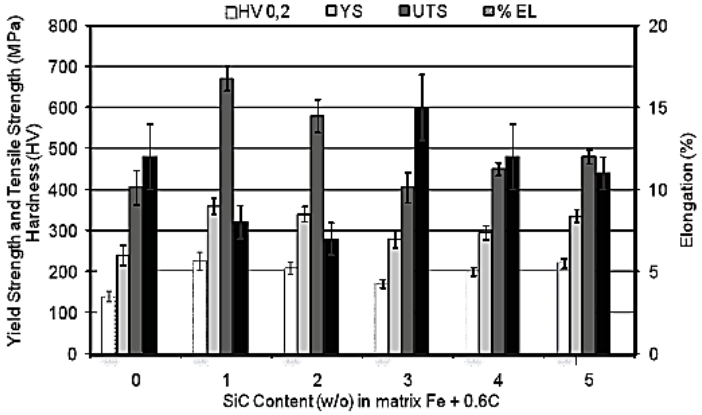

Source: Binder et al. (2010)

Scuffing resistance measures the work that the lubricating layer is able to endure until it looses the ability to lubricate the sliding contact (by breakage of other effects produced by the sliding motion itself). The scuffing resistance presented in fig. 7 was measured by sliding an spherical counter-body against the samples and applying incremental normal forces in steps of 7N until the friction coefficient consistently

surpasses a certain criteria (0.2 for solid lubrication) according to the process developed by De Mello in 2006. As shown by fig. 7 alloys with 1% SiC presents the lower durability of the lubricating layer and the highest friction coefficient (taking the 0% SiC alloy as a base), this occurs because it doesn't have enough lubricant phase (graphite) to maintain the lubricating layer integrity as the counter-body breaks it. The Fig 8 shows how SiC additions to the matrix affects the mechanical properties of the carbon steel by producing solid solution hardening (due both silicon and carbon being dissolved into the matrix) and an increase in the hardenability of the samples.

The figure 9 shows the microstructural aspect of the above mentioned alloys, is noticeable that for SiC contents ≥ 3% the resulting microstructure turns to be almost completely ferritic.

Fig. 9 - Microstructure of Fe + 0.6C + 0-5SiC alloys sintered 1 hour at 1150°C

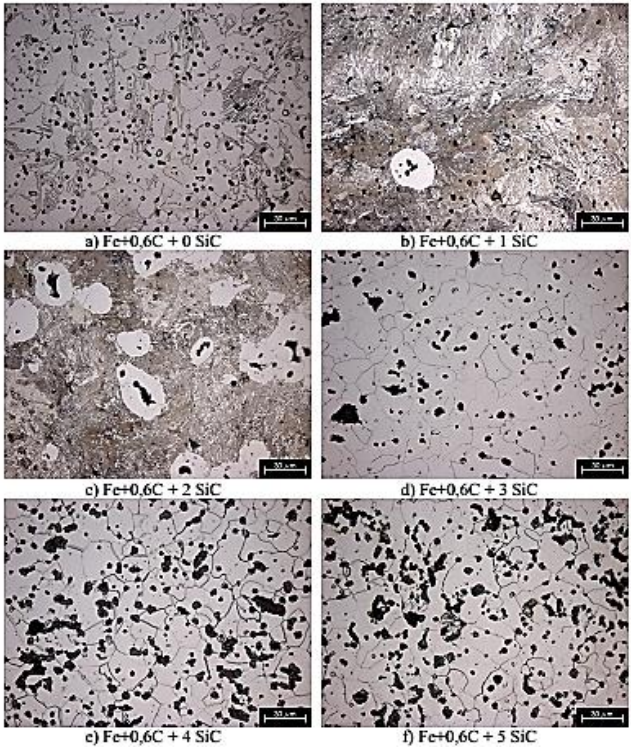

Source: Binder (2009)

The figure 10 shows the effect on scuffing resistance and friction coefficient of Ni and Mo addition on a Fe + 0.6C + 3SiC self-lubricating steel sintered 1 hour at 1150°C.

Fig. 10 - Effect of Ni and Mo additions to a Fe + 0.6C + 3SiC self-lubricating PIM sintered steel

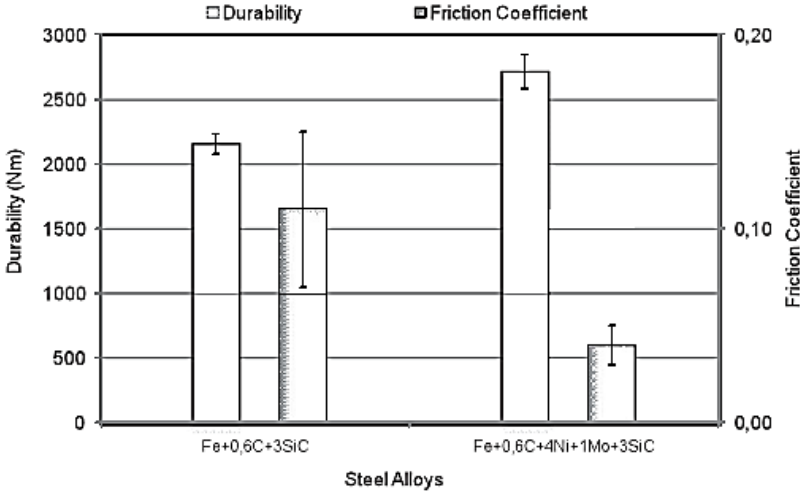

Source: Binder et al. (2010)

Figure 10 shows that Ni and Mo additions have a positive effect in the tribological properties of the self-lubricating steel studied, the reduction of the friction coefficient and the increase on durability are related with the improvement of the mechanical properties of the matrix associated to solid solution hardening and microstructural changes produced by Ni and Mo. SiC quantity influences the Si availability and hence the α stabilizing effect done by Si. As shown in fig 9, for SiC contents of 1% and 2% a low amount of graphite nodules was found due the low availability of SiC in the samples. From a 3% SiC the resulting microstructure consist in ferrite rings with graphite nodules inside (BINDER, 2009). Ni presence on the samples produces the generation of large and compact nodules when compared to those generated in the same conditions without Ni addition (DE MELLO et al., 2013) this is because while Ni is a γ stabilizer it also greatly reduces the diffusion coefficient of Si into the matrix, this causes Si to build up around the graphite nodules during the dissociation of SiC, this build up causes ferrite to precipitate around the ferrite nodules due Si ferrite stabilizing

effect, as carbon have a limited solubility into ferrite (< 0,02 wt%) the graphite nodules generated this way remain rounded without loosing too mucho carbon to the matrix.

Highly stabilized ferritic microstructures (such as ferrite containing a high percent of silicon) have a poor or almost none susceptibility to quenching and tempering heat treatments, however as was found in (DE MELLO et al., 2013) Fe + 0.6C +4Ni +1Mo + 3SiC shows a mixed microstructure of ferrite and austenite derivates such as martensite, bainite and retained austenite. So taking into account all the factors presented up to this point the alloys to be heat threated and characterized will have a Fe + 0.6C + 4Ni + 1Mo matrix and 2 and 3% SiC, using a 0% SiC alloy as comparative basis. All the test specimens will be sintered at 1150 °C for 1hour to achieve SiC dissolution without generating complete homogenization. The next sub-section makes a brief introduction to steel heat treatments.

3.4 HEAT TREATMENT OF STEELS

Steels are commonly defined as ferrous alloys with carbon content between a centesimal percent up to a 2% in mass that could have other alloy elements such as Mn, Cr, Ni, etc. This means that steels can exhibit a wide variety of properties depending on its chemical composition, phases and microconstituents which in time depends on the heat treatments applied on it (HARRY, 1995).

The objective of heat treatments is to improve mechanical properties such as hardness or toughness. To achieve the maximum hardness in low alloy steels the desired microstructure is martensite. Martensite hardness depends on carbon content, however, if the sample's microstructure isn't completely martensitic the final hardness of the treated piece will be lower (ASM INTERNATIONAL HANDBOOK COMMITEE, 1991).

Figure 11 shows a metastable equilibrium diagram for the Fe-C system. If alloy elements are added, the position of A_1, A_3 and A_{cm} lines is changed as so is the eutectoid composition (ASM INTERNATIONAL HANDBOOK COMMITEE, 1991).

Fig. 11 - Metastable equilibrium diagram of the Fe-C system

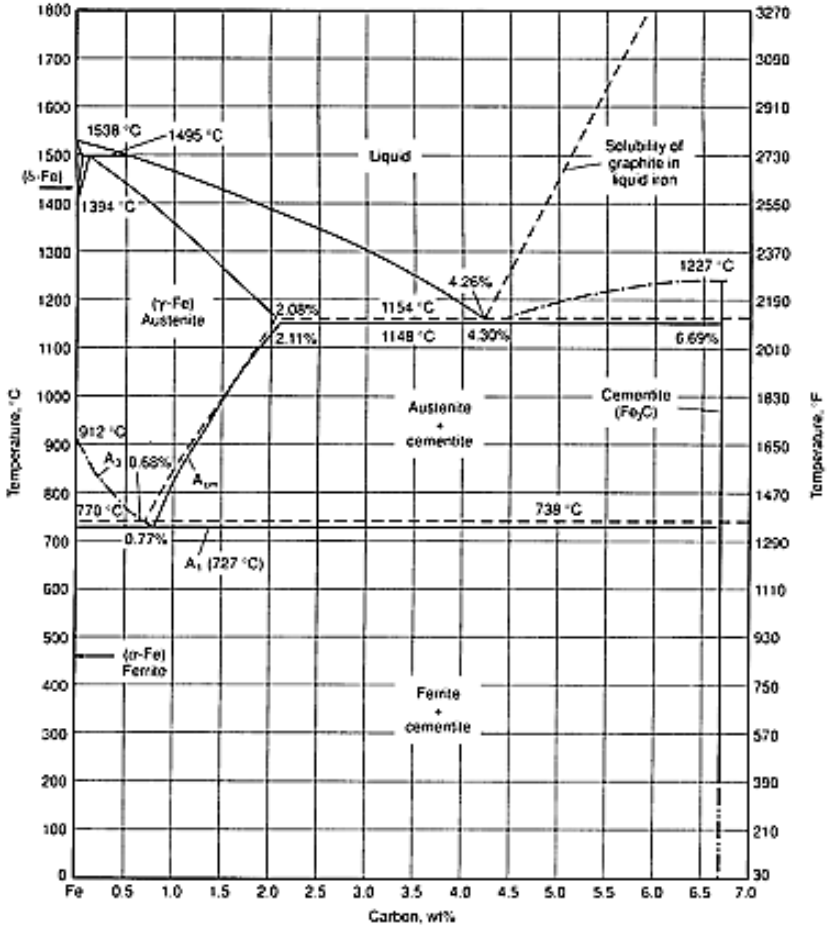

Source: ASM International (1991)

Figure 12 shows the variation of A1 line and eutectoid carbon with the addition of some alloy elements.

Fig. 12 - Alloy elements influence in eutectoid temperature and composition

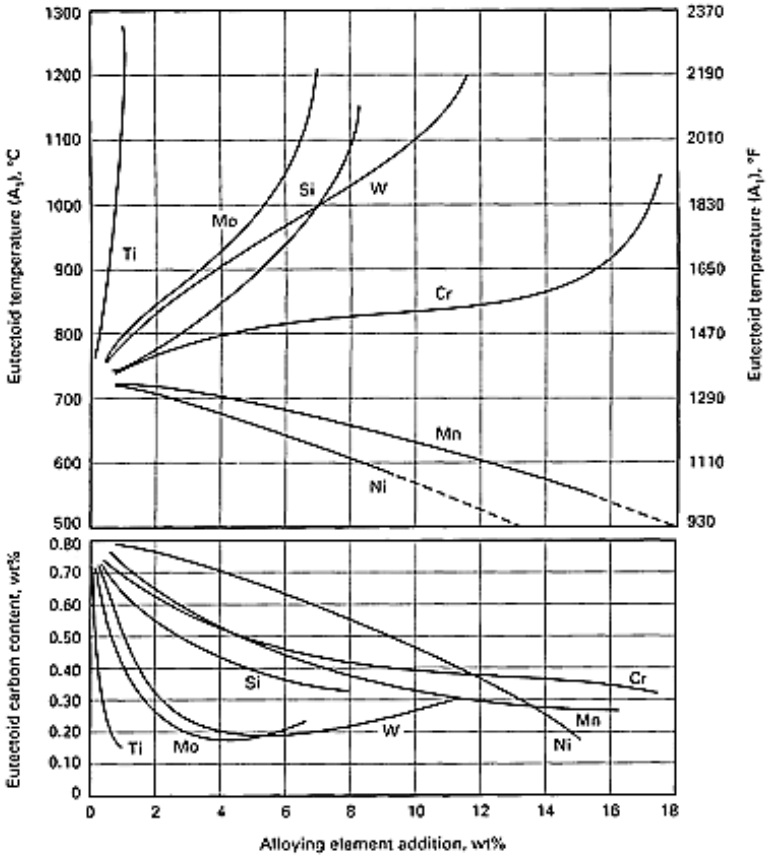

Source: ASM International (1991)

From figure 12 can be noticed that:

- All the alloy elements shown decrease eutectoid's carbon content.
- γ phase stabilizers decrease A_1 temperature.
- α phase stabilizers increase A_1 temperature.

Phase transformations kinetics aspects are as important as equilibrium diagrams for steel heat treatments. Metastable phases

martensite and bainite are generally produced by rapid cooling to room temperature (quenching) or by isothermal decomposition of austenite at relatively low temperatures (but higher than room temperature). If these metastable phases are reheated to moderate temperatures, they are decomposed in more stable mixtures of ferrite and cementite. This process is known as tempering. To predict the microstructural evolution of steel during cooling isothermal transformation (IT) and continuous cooling (CCT) diagrams are used

3.4.1 Isothermal Transformation Diagrams

These diagrams show what occurs when a defined steel piece is maintained at a constant temperature by a prolonged amount of time. Microstructural developing in time can be tracked by having samples treated in lead or salt, quenching them in incremental times and then measuring the phases formed with a microscope (ASM INTERNATIONAL HANDBOOK COMMITEE, 1991). An alternative is to use an unique sample and a dilatometer to record dimensional changes in time produced by microstructural changes in the sample (ASM INTERNATIONAL HANDBOOK COMMITEE, 1998). Figure 13 presents and ITT diagram example for a AISI 4140 steel under two different austenizing conditions.

Fig. 13 - Comparison between IT diagrams for AISI 4140 steel al after 6 s austenizing time at 950 °C (continuous line) and 10 min at 860 °C (dashed line)

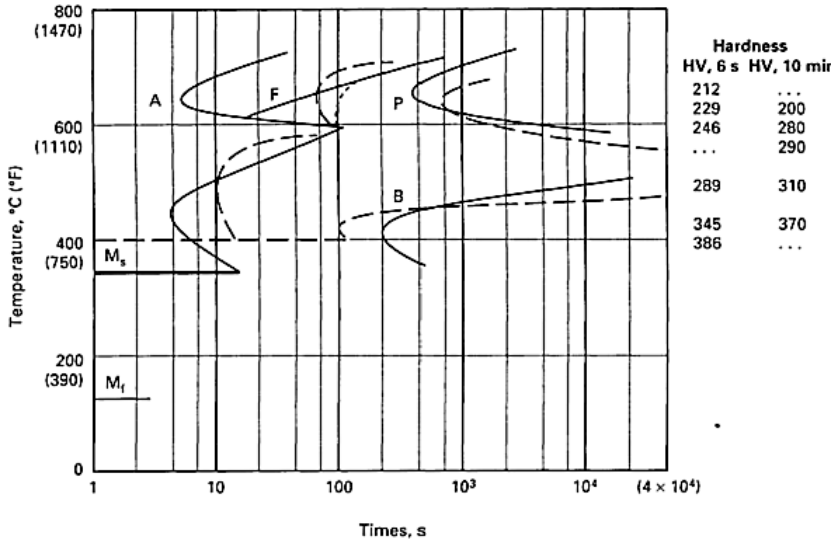

Source: ASM International (1991)

3.4.2 Continuous Cooling Diagrams

The use of isothermal cooling is common for most of experimental research; however this situation isn't just as common in practice. For that reason continuous cooling diagrams (CCT) have been developed. These diagrams can be helpful if the cooling rate of the sample is either known or can be calculated or simulated (ASM INTERNATIONAL HANDBOOK COMMITEE, 1991). Figure 14 shows IT and CCT diagrams for a AISI 4130 steel.

Fig. 14 - Isothermal transformation (upper) and CCT (lower) diagrams for AISI 4140 steel containing. The CT diagrams are computed (dashed lines) and experimentally determined (continuous line)

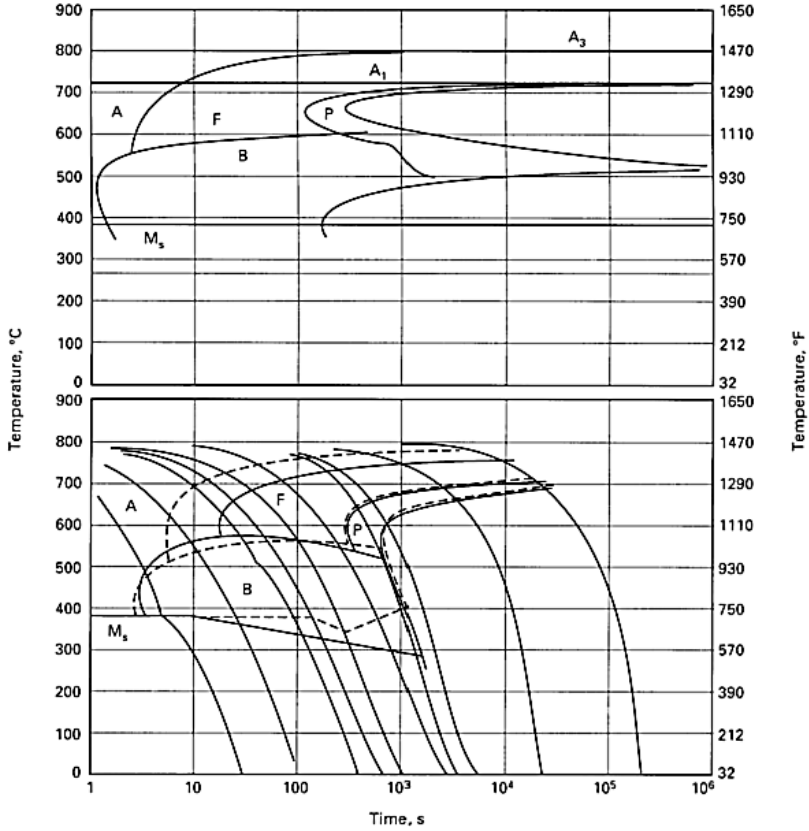

Source: ASM International (1991)

In this work the involved alloy elements were silicon, nickel and molybdenum. Both Mo and Si are elements that stabilize alpha phase and therefore increase the A_1 temperature, Ni however is a gamma phase stabilizer and hence it decreases A1 temperature. In the other hand all three of them lower the carbon content of the eutectoid point; all this was shown back in fig 12. About the transformation diagrams all these alloy elements increase hardenability displacing pearlite formation curves to the right. As both methods of cooling were presented, this

study used isothermal cooling treatments such as martempering + tempering and austempering.

3.4.3 Tempering of Steels

3.4.3.1 Martempering and Tempering

Martempering consist in an interrupted quench from the austenizing temperature of certain alloy, cast, tool or stainless steels. Cooling is delayed just above martensitic transformation in a molten salt or oil bath for the time needed to equalize temperature throughout a piece, for the purpose of minimizing distortion, cracking and residual stress. Cooling to room temperature in air finalizes the process. The resulting microstructure is primarily martensitic and is untempered and brittle (HARRY, 1995).The fig 15 shows differences between conventional quenching and martempering.

Fig. 15 - Differences between conventional quenching + tempering (a), martempering + tempering (b) and modified martempering + tempering (c)

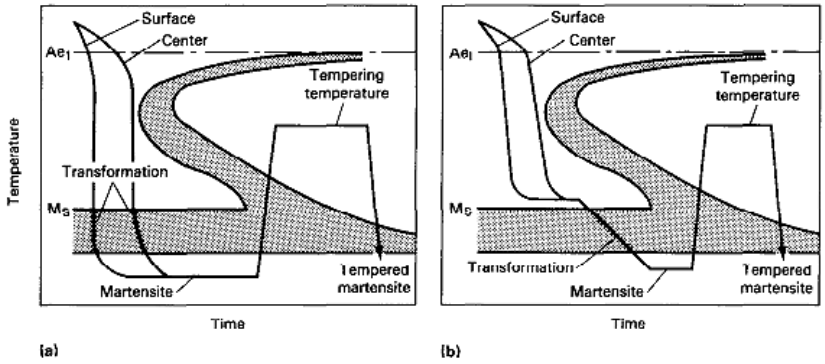

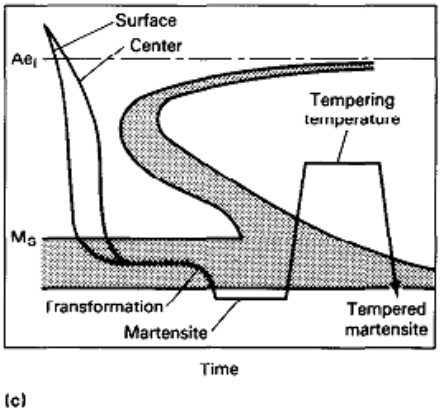

Source: ASM International (1995)

In martempering residual stresses are lower than those developed in conventional quenching because the greatest thermal variations come while the steel is still in its relatively plastic austenitic condition and because final transformation and thermal changes occur throughout a part at essentially the same time (HARRY, 1995).

Other advantages of the process are:

- Susceptibility to cracking is reduced or eliminated
- When the austenitizing bath is a neutral salt and is controlled by the addition of methane or by proprietary rectifiers to maintain its neutrality parts are protected with a residual coating of neutral salt until they are immersed in the martempering bath
- Martempering often eliminates the need for quenching fixtures, which are required to minimize distortion in conventional quenching

The only difference between martempering and modified martempering is the temperature of the quenching bath as it's below that of the M_s point which increases the severity of the quench (see fig 15-c). This capability is important for steels with lower hardenability that require faster cooling to get a great depth of hardness (HARRY, 1995)

Finally tempering is performed after martempering to reduce the fragility of the martensitic phase by isothermally transforming it into a

mixture of ferrite and spheroidized cementite, this can be done in a conventional electric furnace or in a molten neutral salt bath to avoid excessive decarburization and oxidation of the pieces. Fig 16 shows and example of mechanical properties changes associated with tempering temperatures.

Fig. 16 - Effect of tempering temperature on the mechanical properties of an AISI 4340 oil-quenched steel bar.

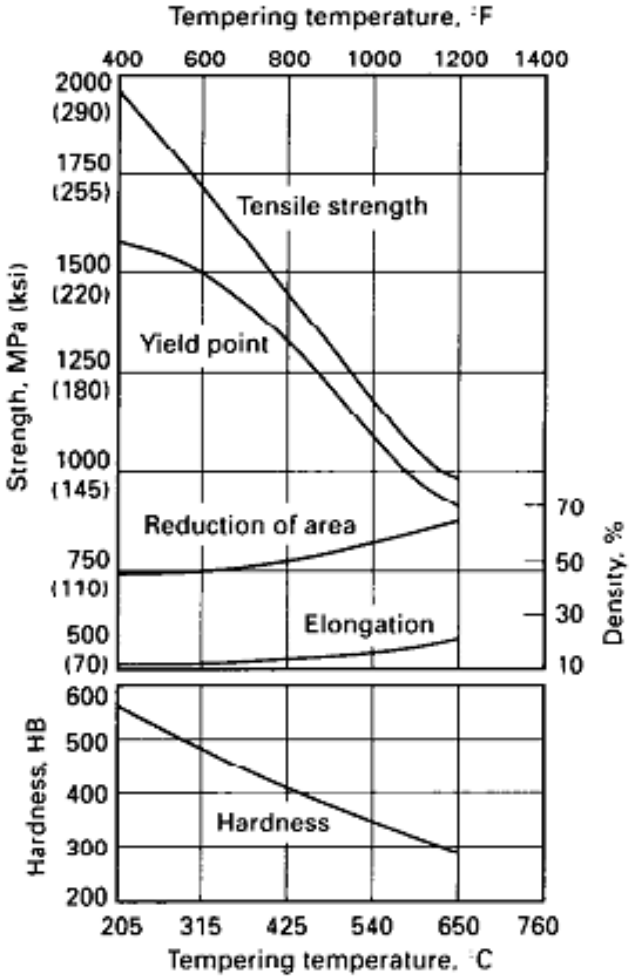

Source: ASM International (1995)

Some strong carbide-forming elements such as chromium, molybdenum and vanadium causes secondary hardening in tempered steel by forming small, dispersed carbides during the martensite decomposition process being more effective in increasing hardness at temperatures above 205°C. Silicon was found to be most effective in increasing hardness at 315°C. The increase in hardness caused by elements like phosphorus, nickel and silicon can be attributed to solid-solution strengthening. Under certain conditions, such as with highly alloyed steels, hardness may actually increase (HARRY, 1995).

3.4.3.2 Austempering

In this process, a ferrous alloy is isothermally quenched at a temperature below that of pearlite transformation but above that of M_s.

Workpieces are heated to a temperature within the austenitizing range, usually 790 to 915 °C. Quenching is done onto a bath maintained at a constant temperature, usually in a range of 260 to 400 °C. Parts are allowed to transform isothermally to bainite in this bath. Cooling to room temperature completes the process (HARRY, 1995)

Fig. 17 shows the differences between austempering and conventional quenching and tempering. In true austempering metal must be coolod from austenitic temperature to the temperature of the austempering bath fast enough to ensure complete transformation of austenite to bainite.

Fig. 17 - Comparison of time-temperature transformation cycles for conventional quenching + tempering and austempering

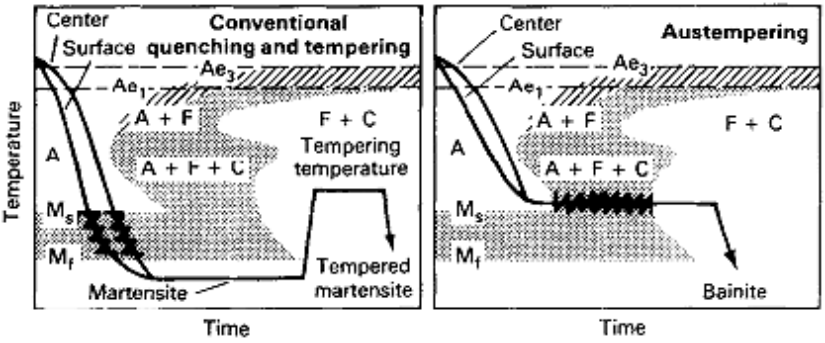

Source: ASM International (1995)

Advantages of austempering include higher ductility, toughness and strength at a given hardness and reduced distortion when compared to martensite based heat treatments.

The most appropriate description of bainite is that the microstructure consist of a non-lamellar mixture of ferrite and carbides, which can be classified further into upper and lower bainite (BHADESHIA, 2001a). This distinction is because there are clear differences in the mechanical properties of upper and lower bainite.

Lower bainite is obtained by transformation at relatively low temperatures. Both upper and lower bainite form as aggregates of small plates of ferrite. The essential difference between them is in the nature of the carbide precipitates. Upper bainitic ferrite is free of precipitation, the carbides present grows from the carbon-enriched residual austenite between the plates of ferrite. In addition to this type of precipitation, there are carbide precipitates in lower bainite's ferrite (BHADESHIA, 1980, 2001a). Fig 18 shows the differences between upper bainite and lower bainite in terms of carbides precipitation.

Fig. 18 - Schematic representation of upper bainite and lower bainite transitions

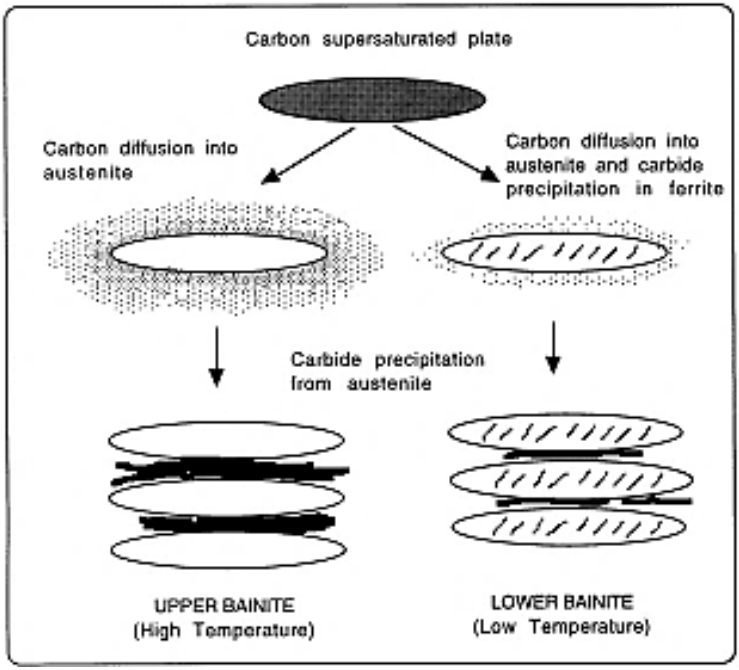

Source: Bhadeshia (2001a)

As for the mechanical properties it should be pointed that lower bainite presents an higher impact toughness with a lower ductile-brittle transition temperature when compared to upper bainite (BHADESHIA, 2001b), also for a determined carbon content it has an higher hardness value when compared with upper bainite as shown in fig 19.

Fig. 19 - Vickers hardness value for pearlite and bainite produced in a 0.69C plain carbon steel.

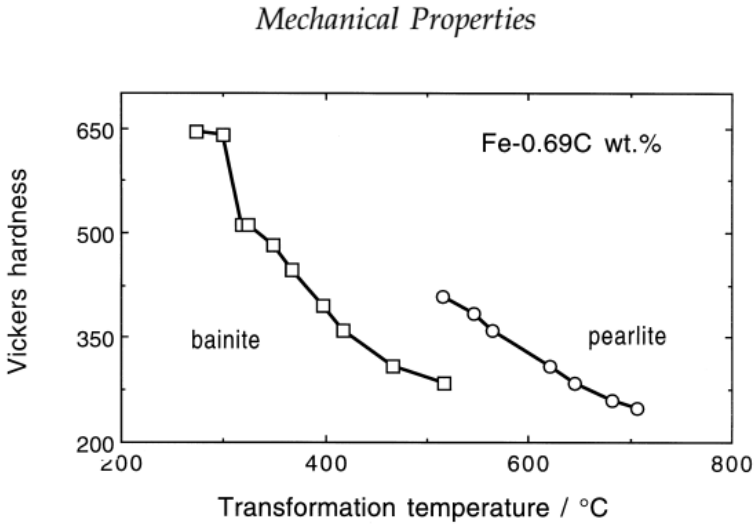

Source: Bhadeshia (2001b)

For the current work an austempering temperature of 300 °C was used for 2 hours to achieve acceptable growth kinetics of lower bainite in a Fe + 0.6C + 4Ni + 1Mo steel matrix. The materials and methods used to determine the heat treatment parameters are discussed in the following chapter.

4. MATERIALS AND METHODS

In this chapter the characteristics of the materials used, the equipment and the characterization techniques used in the current work are introduced. Regarding this Fig. 20 shows a flow diagram of the experimental procedure used in this work.

Fig. 20 – Experimental procedure flow diagram.

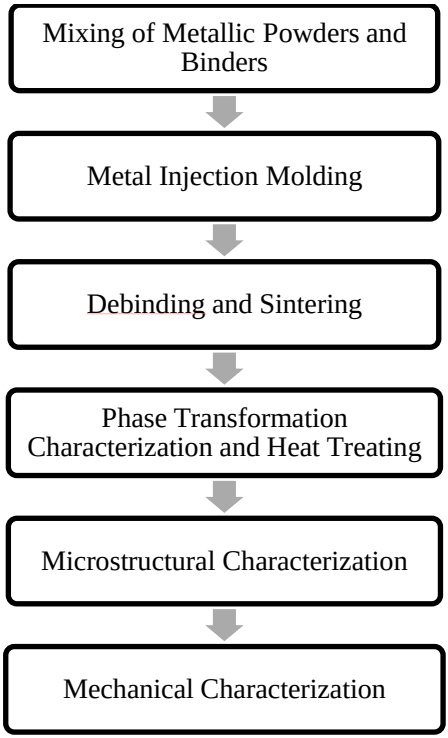

Source: Author.

4.1 RAW MATERIALS

The raw materials used to produce the test specimens are listed below in table 2. Table 3 shows the characteristics of the polymer binder system composed by a mixture of thermoplastic resin, plasticizer, lubricant, surfactant and anti-oxidizer being a 8% of the feed's total mass.

Table 2 - Raw powder materials used

Element	Commercial name	Particle mean size (μm)	Purity (%)	Supplier
Fe	CL-OM	7.84	98,3	Basf
Ni	PF-10F	6.06	99,9	ATMIX
Mo	OMP	5.50	99,8	HC Starck
SiC	800	10.0	99,0	Cobral

Source: Raw materials datasheets.

Table 3 - Binder composition

Element	Mass % of the mixture	% of the constituent in the binder
Polypropylene	3,405	42,56
EVA	1,321	16,51
Paraffin	2,895	36,19
Cocamide DEA	0,363	04,54
Anti-oxidant	0,018	0,20
Total	8,000	100,00

Source: Author.

4.2 POWDER MIXTURE PREPARATION

A pre-mixture step to homogeneously distribute the binder (polyprophilene, paraffin-wax, EVA, Cocamide DEA and antioxidant) into the raw material mixture was manually performed into a single container and then the mixing step was done using a sigma class Haake mixer at 180 °C, 70 RPM for 90 minutes. After the mixing step the now denominated feedstock was crushed using a Seibt blade grinder. The product of the whole process was a load of granules containing a mixture of the raw materials and the binder system with the adequate size to be used in the injection equipment.

4.3 POWDER INJECTION MOLDING

After feedstocks preparation the test specimens were injected. For tensile test, tensile test specimens were injected according to MPIF 50 standard, its geometry is shown in figure 21 (a). For microstructural characterization and hardness and micro hardness measurements bowtie specimens were produced as shown in figure 21 (b).

Fig. 21 - Test specimens: (a) Tensile tests (b) Other tests

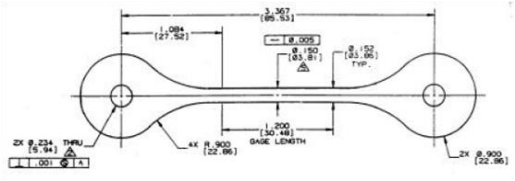

(a)

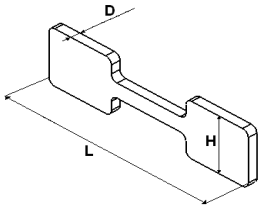

H=19,00 mm;D=3,00 mm;L=69,80 mm
(b)

Source: Adapted from Binder, (2009)

The equipment used for powder injection molding of the test specimens was an Airburg 320S with a closure force of 50 tf and the main parameters used during the injection process are listed in table 4.

Table 4 - Powder Injection Molding processing parameters

Injection Pressure (bar)	1000
Settlement Pressure (bar)	800
Injection Temperature (°C)	180

Source: Author.

4.4 DEBINDING AND SINTERING.

The multicomponent binder system as described in table 3 requires a two-step debinding process in order to achieve optimal removal of the polymeric components. The first step was chemical dissolution of the lower molecular weight components of the binding system using hexane ($CH_3(CH_2)_4CH_3$) heated at 55 °C, first by exposing the samples to the hexane vapor 2 hours and then by immersing the samples into the hexane bath 6 hours. This two-step chemical debinding can be explained as follows: when the specimens are exposed to hexane vapor, the more soluble elements starts to dissolve, leaving fine conduits in the form of pores. When the specimen is then immersed into the bath the solvent easily penetrates the sample up to the core due the existing pore channels. As the solvent penetrates the sample, the existing channels broaden and new pores start to grow. This situation persists until all the soluble binder is extracted during this step.

To remove the component with higher molecular weight (namely polypropylene) plasma assisted debinding and sintering process was used (PADS). The PADS process was done under controlled heating conditions using an hydrogen flux of 1000 cm^3/minute up to 500 °C. Then a 500 cm^3/minute flux was used which consisted into a mixture of 95% argon (99.999% purity) and 5% hydrogen (99.995% purity). Operational parameters of the complete process are listed in table 5.

Table 5 - Processing parameters for the Plasma Assisted Debinding and Sintering step

Temperature (°C)	Heating rate (°C/minute)	t_{on} (μs)	Gas flux (%)		Pressure (torr)
			H2	Ar	
T_{room} to 300	7.0	50	100	-	1
300 to 500	1.0	100	100	-	1
500 to 1150	5.0	50	5	95	1
1150	1 hour sintering	50	5	95	1
Cooling	-	50	5	95	0.5
Voltage (V)	400				

Source: Author

The sintering temperature and time were chosen from the findings exposed by Binder in 2009 as they proved to be good parameters to obtain low porosity (< 4%), high mechanical properties and a high amount of SiC dissociated without achieving complete dissolution.

4.5 HEAT TREATING

Four different conditions/heat treatments were considered for the current work.

1. As Sintered condition: The initial condition of all the sintered specimens, it consist into cooling the samples inside the reactor when the sintering process is finished, is characterized for its low cooling rate which behaves in a decreasing logarithmical way, the PADS reactor takes 3 hours to reach 200°C so it can be shut down, the rest of the cooling occurs overnight in a vacuum environment until the samples are finally extracted the day after.
2. Martempered and tempered at 300°C: These test specimens were austenized and quenched into a salt bath at 180 °C for 20 minutes, then they were air cooled to room temperature and tempered in a salth bath 2 hours at 300 °C.
3. Martempered and tempered at 530 °C: These test specimens were austenized and quenched into a salt bath at 180 °C for 20 minutes, then they were air cooled and tempered 2 hours at 530 °C.
4. Austempered: These test specimens were austenized and then austempered into a salt bath 2 hours at 300 °C.

The austenizing parameters for treatments 2,3 and 4 were 20 minutes at 880 °C, the time was chosen according to ASM Heat Treater's Guide (HARRY, 1995).

4.6 CHARACTERIZATION

4.6.1. Differential Dilatometry

Differential dilatometry was used to analyze phase changes at heating and cooling. For these tests: samples taken from sintered tensile test specimens were used, with dimensions of 4.8 x 10 mm (diameter x height). The tests conditions were: Heating at 10 °C/min up to 950°C, then a 20 minutes step at 950 °C and then cooling at 10 °C/min up to 100 °C into an atmosphere of 95% Ar-5% H2.

4.6.2. Metalographic Preparation

Metallographic samples were cut using a BUEHLER ISOMET 4000 precision cutter with a low density diamond saw. Immediately the samples were mounted into epoxy resin and then sanded and polished. The microstructure was revealed using Nital 2% (98 ml alcohol and 2 ml nitric acid) and Picral 4% (100 ml alcohol + 4 grams of picric acid).

4.6.3. Optical Microscopy

The optical images were obtained using a Leica DM4000 microscope coupled with a Leica DC 300 digital camera. The images were white balanced and digitalized using LAS v4.5 software, the resolution of the images was 2560 x 1920 pixels.

4.6.4. Scanning Electron Microscopy

Characterization of the cross-section of the specimens in terms of size and composition of microstructural constituents was done by using SEM microscopes.

a) Conventional scanning electron microscope (SEM) model JEOL JSM-6390LV with tungsten filament, accelerating potential from 0.5 to 30kV and benchtop SEM HITACHI TM3030. Chemical composition was obtained using an energy dispersive spectrometry microprobe coupled with the SEM. Superficial images were obtained using the secondary electron (SE) detector at different magnifications.

b) Field emission gun (FEG) SEM, model JEOL JSM-6701F. With cold cathode, ultra vaccum and high resolution: 1nm (30kV) – 2.2n (1.2kV). Acceleration potential varying from 0.5 to 30 kV and magnification from 25x to 650000x.

4.6.5. Hardness.

Hardness measurements were done using a 2.5 diameter tungsten sphere according to ISO 6506 standard. The machine used for testing was an EMCO-TEST M4C/R. 10 indents were used to attain a hardness value in each sample tested.

4.6.6. Micro-Hardness

Micro hardness tests were performed using Vickers scale according to ASTM E386 standard, the applied load was of 10g. The equipment used was a Shimatzu HMV 2000.

4.6.7. Tensile Tests

Tensile tests were performed according to ISO 6892 standard. The equipment used was a Zwick/Roell testing machine. The test specimens had a gauge length of 35 mm and mean diameters of 4.8 mm. 3 tensile specimens were used in each test.

5. RESULTS AND DISCUSSION

In this chapter mechanical and microstructural properties obtained as result of sintering and heats treating of the samples are exposed. Phase transformations and its correlations with chemical and mechanical properties of the studied alloys are discussed.

5.1 HEAT TREATMENTS

To determine the parameters for heat treatments software simulations and dilatometric measures were used, A_1 and A_3 temperatures were determined directly from dilatometric result and non-equilibrium parameters such as M_S, B_S and B_F were estimated using ASM STECAL 3.0.3 software.

5.1.1 Dilatometry and CCT diagrams

Dilatometric test were performed on the three alloys in the as-sinter condition. The samples were heated up to 950°C and then cooled to 100°C, both heating and cooling rates were set to 10 °C/min. Figs 22 and 23 shows dilatometric curves for heating and cooling for the three alloys respectively.

Fig. 22 - Heating dilatometric test for Fe+ 0.6C +4Ni + + 1Mo with variable SiC%

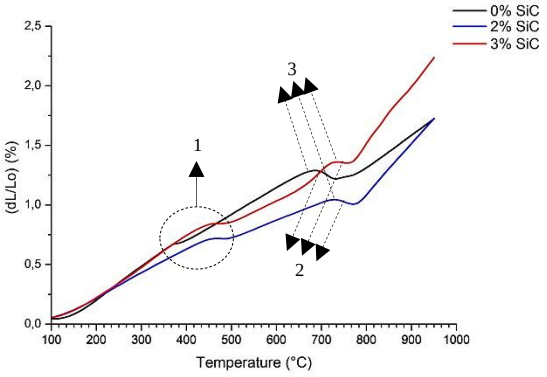

Source: Author

From the heating dilatometric curves several things should be noticed:

1- The samples undergo a previous transformation prior to carbide dissolution and ferrite transformation into austenite: This can be explained by a partial tempering process as a result of martensite present in the as sintered samples.
2- SiC content decreases the severity of the volumetric change from ferrite to austenite: as part of the microstructure of the SiC containing alloys is highly stabilized ferrite hence, if doesn't transform into austenite in the A_1-A_3 range. This is particularly noticeable in the samples containing 3 wt% SiC where the A_1-A_3 range appears as an almost flat line rather than a "bump" when compared to the other two samples.
3- A_1-A_3 temperatures are influenced by the Si dissolved in the matrix product of the SiC dissolution during sintering: as Si difficult the transformation of ferrite into austenite, a rise in the transformation temperatures A_1 and A_3 is expected.

Table 6 shows the A_1-A_3 temperatures determined for all the three samples.

Table 6 - Austenite transformation temperatures for Fe + 0.6C + 4Ni + 1Mo Sintered steel with variable amount of SiC

	0% SiC	2% SiC	3% SiC
A_1 (°C)	685	725	735
A_3 (°C)	730	770	755

Austenite dissociation into ferrite and carbides was studied by cooling down the samples at a rate of 10°C/min as presented in figure 23.

Fig. 23 - Cooling dilatometric test for Fe+ 0.6C +4Ni + + 1Mo with variable SiC%

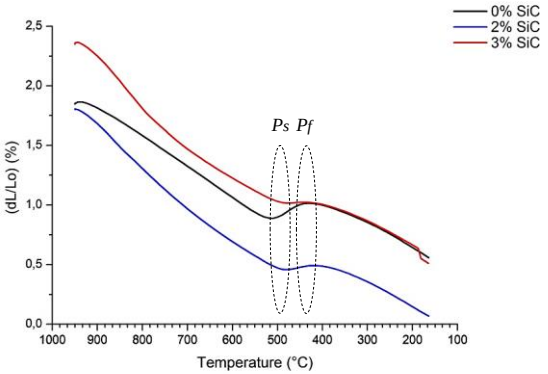

Source: Author

The cooling curve shows the same inverse relationship between the extent of the volumetric change $\gamma \leftrightarrow \alpha$ + carbides and the quantity of SiC (and hence, dissolved Si) in the material. The table 7 shows the P_S and P_F temperatures obtained from the curves above.

Table 7 - Austenite dissociation temperatures for Fe + 0.6C + 4Ni + 1Mo sintered steel with variable amount of SiC

	0% SiC	2% SiC	3% SiC
Ps (°C)	515	480	475
Pf (°C)	425	420	440

Continuous cooling diagrams (CCT) were simulated for the Fe + 0.6C + 4Ni + 1Mo base alloy using the ASM Stecal 3.0.3 software. Fig 24 shows the simulated diagram and the thermal cicles corresponding to sintering and to the heat treatments of martempering and austempering used in the current work.

Fig. 24 - Simulated CCT diagram for base alloy

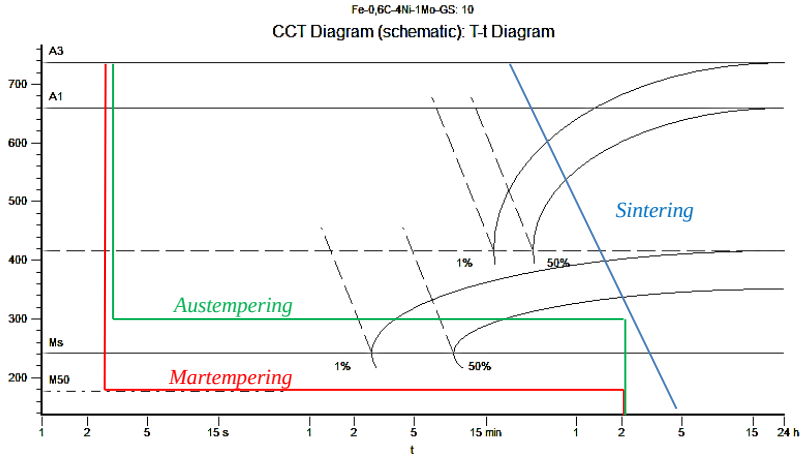

Source: ASM Stecal 3.0.3

The software reports A_1-A_3 temperatures for this alloy of 659-723 °C which are reasonably close to the 685-730 °C obtained by dilatometry. Therefore the heat treatments parameters were chosen taking into account both the experimental and simulated results plus a margin to ensure the occurrence of the desired transformations, as can be seen in the diagram by martempering at 180°C the expected microstructure would be 50% martensite, this is further increased by the 2 hours step and cooling to room temperature. For austempering what's expected is to have at least 50% bainite

5.2 MECHANICAL PROPERTIES

Once the test specimens were heat treated, tensile and hardness tests were performed in order to characterize the material and the influence of SiC content and heat treatments in the mechanical properties of these alloys. The strain hardening behavior is also documented and discussed in this chapter.

5.2.1 Tensile And Hardness Values

Figs. 25 – 27 show the tensile tests results and Brinell hardness measures for Fe + 0.6C + 4Ni + 1Mo sintered steel containing 0, 2 and 3 wt% SiC.

Fig. 25 - Tensile test and hardness results for Fe + 0.6C + 4Ni + 1Mo sintered steel in the As Sintered and heat treated conditions

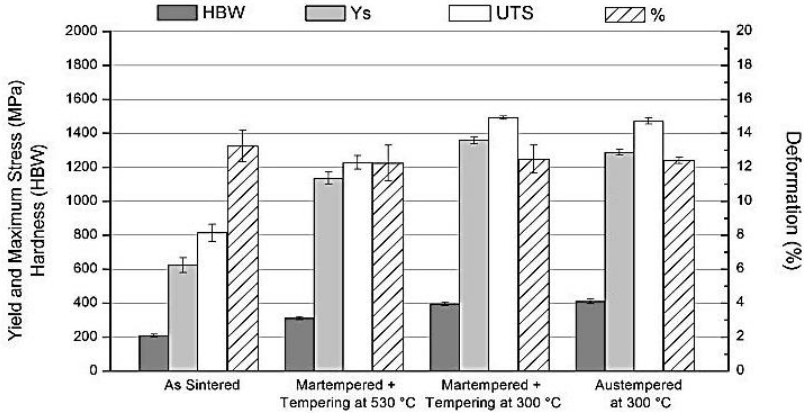

Source: Author.

For the base alloy, mechanical properties such as Y_S, UTS and hardness behave as expected. The as-sinter samples presents high ductility and low mechanical resistance while the martempered and austempered samples exhibits greater mechanical resistance but sacrificing ductility, the austempered samples have a behavior “in-between” the samples tempered at 300 and 530 °C in what respects to tensile properties but shows slightly higher hardness than the sample martempered and tempered at 300 °C.

Fig. 26 – Tensile test and hardness results for base alloy + 2 wt% SiC sintered Steel in the As Sintered and heat treated conditions

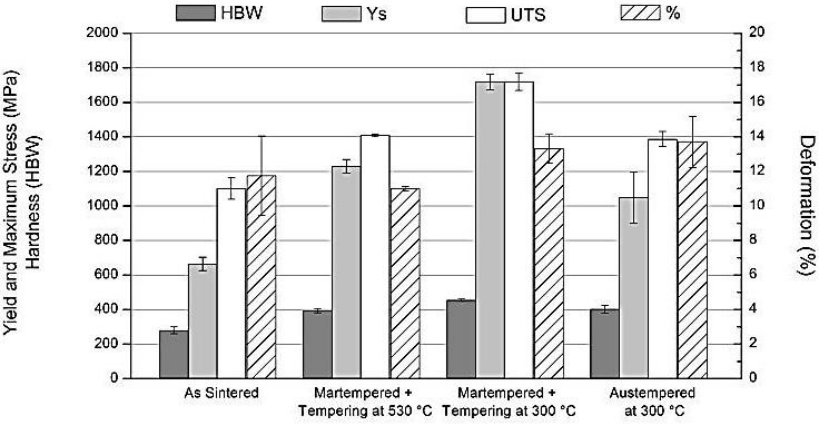

Source: Author

With the addition of 2 wt% SiC the heat treatment effect on the mechanical properties changes, for this alloy the samples martempered and tempered at 300°C shows higher yield strength, tensile strength, hardness and deformation than the samples tempered at 530°C. The austempered samples show higher deformation and lower yield and tensile strength with hardness between the two martempered samples.

Fig. 27 - Tensile test and hardness results for base alloy + 3 wt% SiC sintered Steel in the As Sintered and heat treated conditions

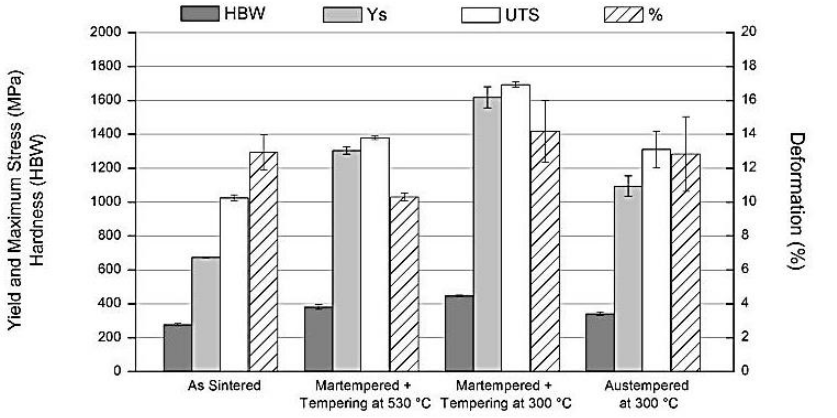

Source: Author

With the addition of 3 wt% of SiC the overall behavior of the previous alloy is conserved. The samples tempered at 300 °C have higher yield and tensile strength than the samples tempered at 530 °C but remain with higher deformation while the austempered samples now shows mechanical properties in between the As Sintered and the martempered and tempered at 530 °C samples. The higher hardness and mechanical resistance of the samples tempered at 300 °C follows the behavior of the base alloy and can be explained by the higher amount of untempered martensite due to the lower tempering temperature, the higher deformation compared to the other samples may be explained by its higher tensile strength which allows the pieces to undergo more elastic deformation until the fracture. The true plastic deformation will be discussed in the next section.

To illustrate the influence of the SiC content in the mechanical properties of these steels fig. 28 shows the above results comparing the SiC additions influence for each condition.

Fig. 28 - Tensile test and hardness results for each condition and alloy

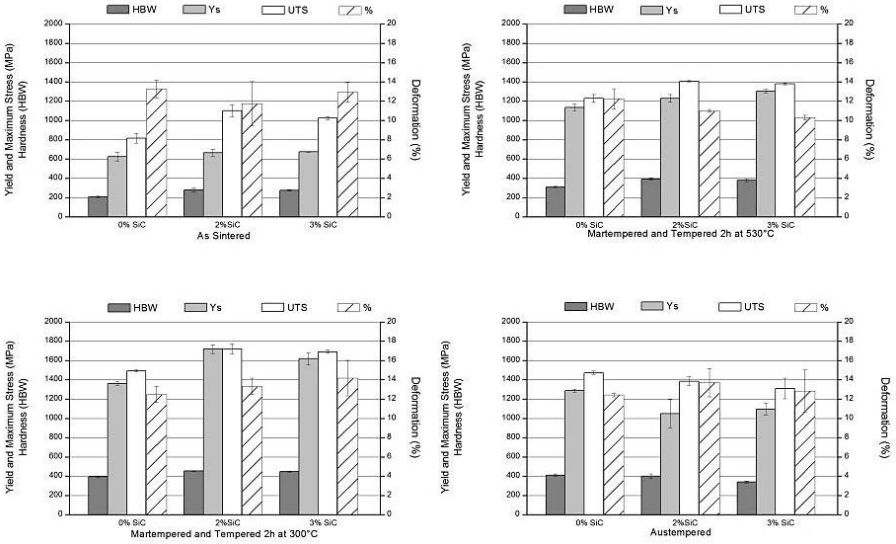

Source: Author

In general terms the additions of SiC to the base alloy improves its mechanical properties by increasing its hardness and mechanical strength without a considerable decrease in ductility. It should be noticed that there are many effects that have to be considered, at one hand the SiC additions adds dissolved Si to the matrix causing solid solution hardening, also the zones with a high amount of Si remains ferritic which is a ductile but soft microstructure, finally the additions of SiC increases the amount of volume consisting in graphite and pores as will be discussed in the microstructural characterization chapter; mechanically graphite nodules behaves as pores due its low shear strength being its presence detrimental to the mechanical properties.

For the austempered samples the trend is reversed, without great differences in ductility the hardness and mechanical resistance decreases with SiC additions. This on principle contradicts the fact that Si additions into bainite produces an increase in the hardness and mechanical properties as stated in (BHADESHIA, 2001b) and reported by (CAI et al., 2011). However, as the same austempering treatment was performed in the three steel alloys disregarding in SiC content, Si dissolution into the matrix may have caused a deviation on the bainite formation kinetics, therefore resulting in different microstructures with different properties when compared to the base alloy. This will be further discussed in the following chapters.

5.2.2 Strain Hardening

Several strain hardening models have been developed to fit experimental stress – strain data into a mathematical model where one or more strain hardening exponents can be extracted (HERTELÉ; DE WAELE; DENYS, 2011). The Hollomon equation is regarded as the most simple and practical way to obtain this parameter even being the method chosen by the ASTM International in their standard (ASTM INTERNATIONAL, 2007). The Hollomon strain hardening exponent (n) is calculated according to equations 1, 2 and 3:

$$\sigma = K\varepsilon^n \quad (1)$$

Where; True Stress $\sigma = S(1 + e)$ (2)

True Strain $\varepsilon = \ln(1 + e)$ (3)

Being S the engineering stress and e the engineering strain. However deviations from this behavior had been reported at low and high strains (KIM et al., 2013; ZHANG et al., 2006). Nevertheless calculations of instant n values over true strain has proven to be a good method to analyze the behavior of steels with mixed microstructures (ZHANG; DING; MISRA, 2015).

The instant strain hardening exponent (n) is calculated as the slope of the curve Log (σ) = nLog(ε) + Log (k) for each value of ε. Figure 29 a, b and c shows the instant strain hardening exponent for Fe + 0.6C + 4Ni + 1Mo sintered steel with additions of 2 and 3% SiC under as sinter, martempered and tempered at 300°C, martempered and tempered at 530°C and austempered conditions.

Fig. 29 - Instantaneous strain hardening exponents (n) v/s true strain for: (*a*) Base alloy, (*b*) Base alloy + 2% SiC and (*c*) Base alloy + 3%SiC

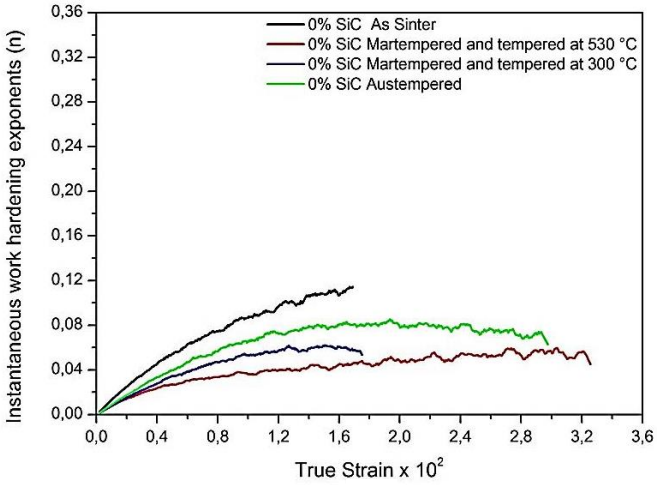

a

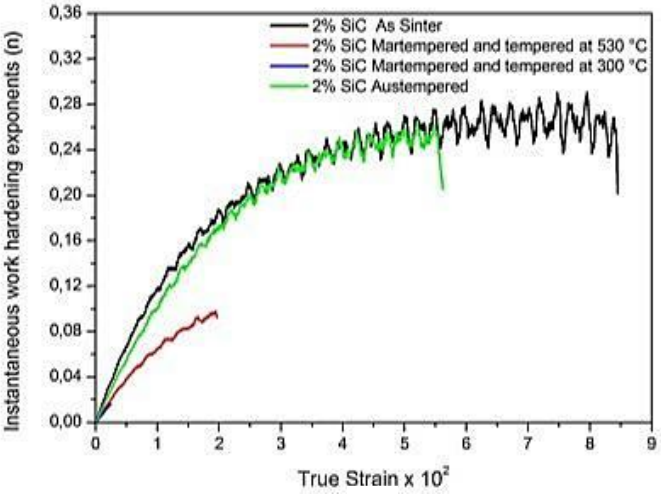

b

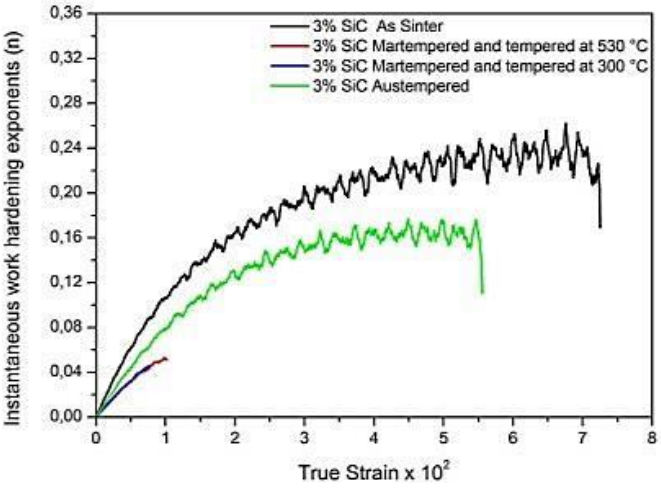

c

Source: Author

From the figures it should be noticed that:

- The steels with additions of SiC exhibits in general larger plastic strain and strain hardening than the base alloy due to the presence of ductile ferrite as a byproduct of SiC dissociation.
- The As Sintered and austempered samples shows larger strains and strain hardening exponents than the martempered samples, SiC additions greatly increases these differences.
- Plastic strain behavior of austempered samples compared with the As Sintered conditions is affected by SiC content, this can be related with the influence of dissolved Si in the microstructure of the austempered samples as previously discussed.

As an high strain hardening coefficient have been reported to positively influence the wear resistance under dry sliding conditions of ferrous alloys containing graphite nodules (BEDOLLA-JACUINDE et al., 2015) while decreasing the friction coefficient (STRAFFELINI et al., 2011) this analysis should be considered of relevance for future research.

5.3 MICROSTRUCTURAL CHARACTERIZATION

To characterize the microstructure obtained by heat treating in the studied alloys, Optical and Scanning electron microscopy was used; this was also complemented with Energy Dispersive X-Ray Spectroscopy and HV 0.1 and HV 0.01 micro hardness measures.

As was found by Binder in 2009, porosity in steels processed by PIM + PADS is unavoidable, also the presence of graphite contributes to this effect as it low shear module and density makes it to behave like pores when it comes to mechanical testing and density measures. Figure 30 show the pores + graphite nodules percent in volume as function of sintering temperature (1 hour) and SiC content.

Fig. 30 - (Pores + nodules) volumetric % of Fe + 0.6C alloys with increasing SiC contents sintered at different temperatures for 60 min

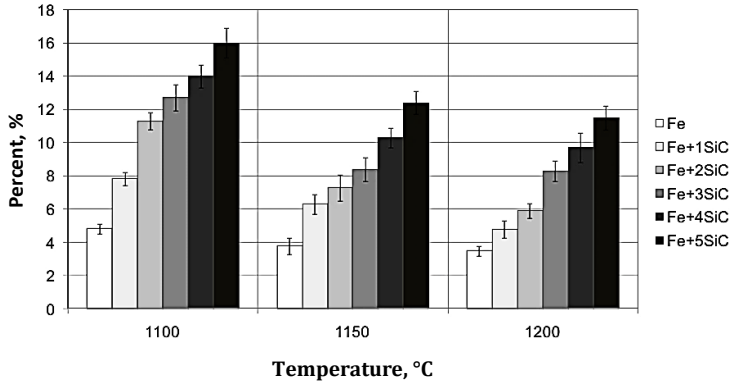

Source: Adapted by the author of Binder (2009).

The presence of pores and graphite nodules, while not easy to optically distinguish one from another, must be considered as it influences mechanical properties such as elastic modulus and yield strength (BRIS CABRERA, 2006; BUCH; GOLDSCHMIDT, 1969; FERNÁNDEZ CASTAÑÓN, 2014) and tribological properties (DUBRUJEAUD; VARDAVOULIAS; JEANDIN, 1994; ROHATGI; RAY; LIU, 1992).

Figure 31shows the microstructure at 200X of the base alloy Fe + 0.6C + 4Ni + 1Mo under as sintered and heat treated conditions.

Fig. 31 - Optical microscopy at 200X of Fe + 0.6C + 4Ni + 1Mo under As Sintered and heat treated conditions. The As Sintered samples were etched with Picral 4 wt% and the heat treated samples were etched with Nital 2 wt%

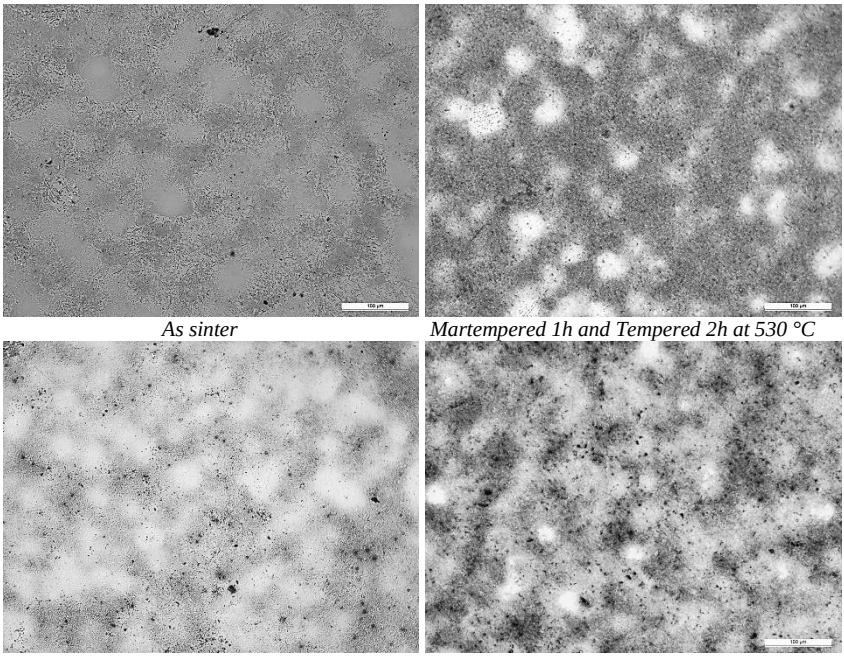

As sinter *Martempered 1h and Tempered 2h at 530 °C*

Martempered 1h and Tempered 2h at 300 °C *Austempered 2h at 300 °C*

Source: Author

The as-sinter samples were etched with Picral reagent as it presents a microstructure of fine dispersed carbides. $HV_{0.1}$ hardness tests were performed into the etched and unetched regions of the microstructure. The etched regions (ferrite + carbides) had a $HV_{0.1}$ hardness of 289 ± 27.8 Vickers and the unetched regions had a $HV_{0.1}$ hardness of 446 ± 51.3 Vickers, this may correspond with a region of untempered martensite and retained austenite (as hardness doesn't correspond with pure 0.45% carbon martensite). These unetched regions are common for all the alloys and conditions studied.

SEM and EDS line scans were performed in the as sintered sample to analyze the difference between etched and unetched regions.

Figure 32 shows the results of EDS line scan over the abovementioned regions

Fig. 32 - Optical microscopy at 1000X of Fe + 0.6C + 4Ni + 1Mo under As Sintered and heat treated conditions

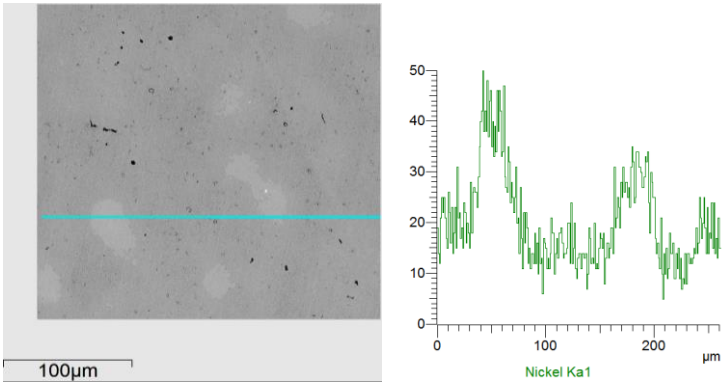

Source: Author

Overall Ni content in the scan was of 3.98 wt% which is practically the Ni content added in the powder mixture however, the unetched areas shows Ni intensity peaks, this suggest incomplete dissolution of Ni into the matrix and hence, zones with higher amounts of Ni may have an higher hardenability and capacity to retain austenite. To better understand the microstructure of these alloys, figure 33 shows the microstructures previously presented at 1000X.

Fig. 33 - Optical microscopy at 1000X of Fe + 0.6C + 4Ni + 1Mo under As Sintered and heat treated conditions

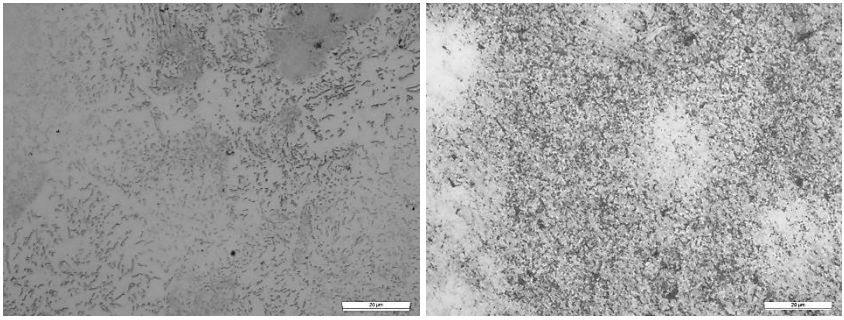

As sinter *Martempered 1h and Tempered 2h at 530 °C*

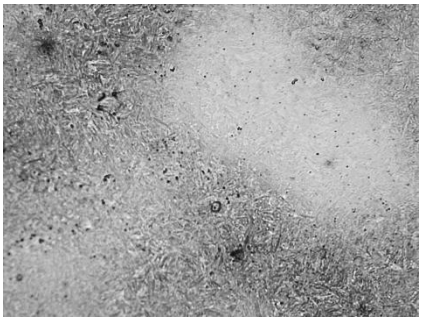

Martempered 1h and Tempered 2h at 300 °C

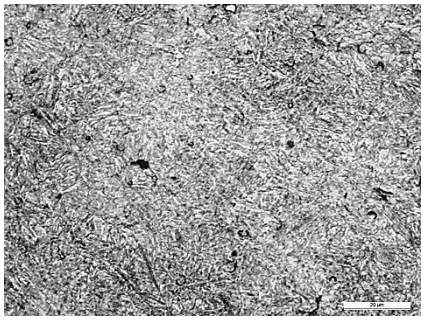

Austempered 2h at 300 °C

Source: Author

The microstructure of the As Sintered samples consists in a fine dispersion of carbides into a ferritic matrix combined with small martensitic zones, as it was previously discussed. This explains the higher plastic strain and strain hardening when compared to the martempered samples. The martempered and tempered samples both presents a mixture of tempered and untempered martensite, it has to be taken into account that in this case untempered martensite can be present due both nickel segregation and partial tempering in the regions with lower amounts of nickel. This is visible as zones with a high amount of nickel appear brighter. The austempered samples show a coarser microstructure with fine dispersed carbides which may correspond to lower bainite.

Figure 34 shows the changes of microstructure with the addition of 2 wt% SiC to the base alloy.

Fig. 34 - Optical microscopy at 200X of Fe + 0.6C + 4Ni + 1Mo + 2SiC under As Sintered and heat treated conditions. The As Sintered samples were etched with Picral 4 wt% and the heat treated samples were etched with Nital 2 wt%

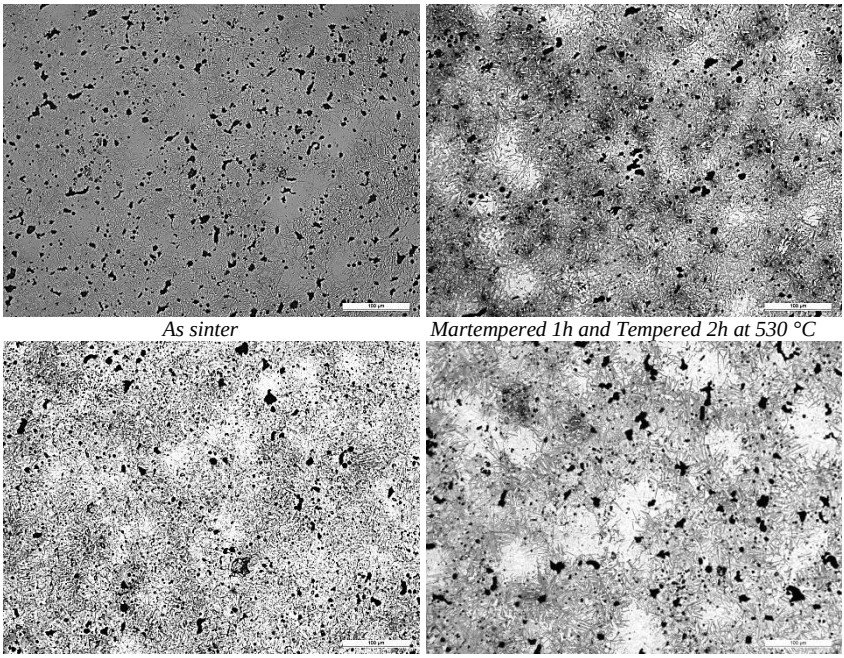

As sinter *Martempered 1h and Tempered 2h at 530 °C*

Martempered 1h and Tempered 2h at 300 °C *Austempered 2h at 300 °C*

Source: Author

The As Sintered samples exhibits the same arrangements of fine carbides into a ferritic matrix and unetched zones with segregated nickel but also presents unetched regions close to the graphite nodules, this is noticeable when etching with picral reagent as it etches carbides preferably. The martempered samples show tempered martensite microstructure and some areas resembling a bainitic microstructure rather than martensitic. This can be explained as Si promotes the ferrite nucleation from retained austenite (CAI et al., 2011) and therefore, equiaxial ferrite laths can be expected to nucleate in the Si rich areas next to the graphite nodules.

Samples with 3 wt% SiC follows the same trend as the samples with 2 wt% SiC. In this regards figure 35 shows optical micrography

images at 1000X of samples with additions of 2 wt% and 3 wt% SiC under As Sintered and heat threated conditions.

Fig. 35 - Optical microscopy at 1000X of Fe + 0.6C + 4Ni + 1Mo + 2SiC and Fe + 0.6C + 4Ni + 1Mo + 3SiC under As Sintered and heat treated conditions. The As Sintered samples were etched with Picral 4

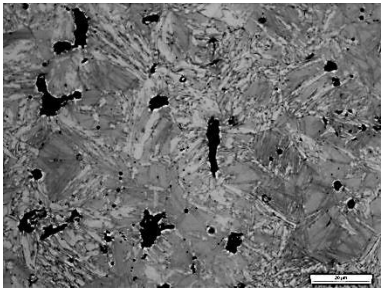

Fe + 0.6C + 4Ni + 1Mo + 2SiC As Sinter

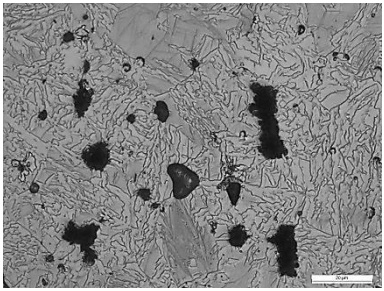

Fe + 0.6C + 4Ni + 1Mo + 3SiC As Sinter

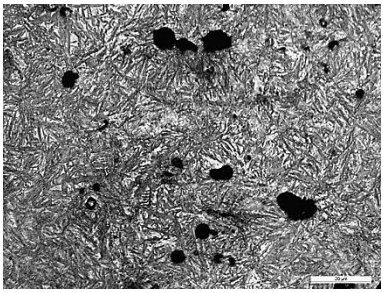

Fe + 0.6C + 4Ni + 1Mo + 2SiC Martempered 1h and Tempered 2h at 530 °C

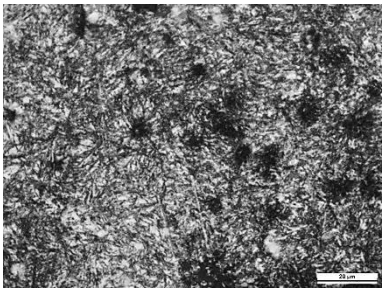

Fe + 0.6C + 4Ni + 1Mo + 3SiC Martempered 1h and Tempered 2h at 530 °C

wt% and the heat treated samples were etched with Nital 2 wt%

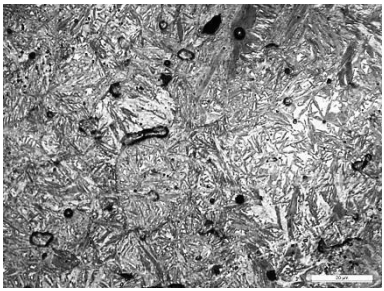

Fe + 0.6C + 4Ni + 1Mo + 2SiC Martempered 1h and Tempered 2h at 300 °C

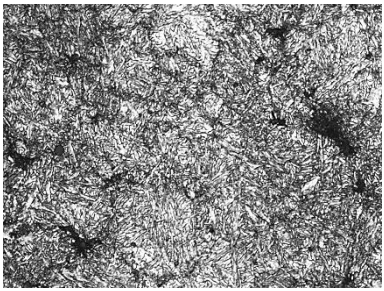

Fe + 0.6C + 4Ni + 1Mo + 3SiC Martempered 1h and Tempered 2h at 300 °C

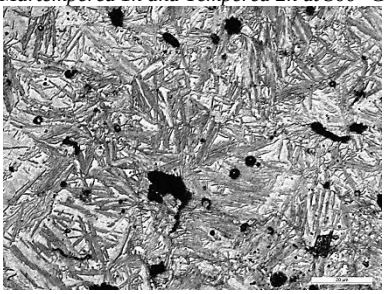

Fe + 0.6C + 4Ni + 1Mo + 2SiC Austempered 2h at 300 °C

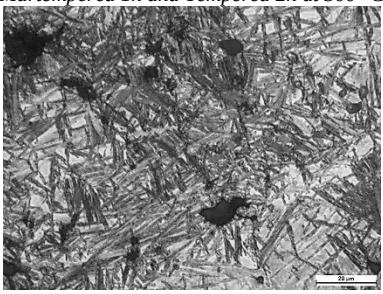

Fe + 0.6C + 4Ni + 1Mo + 3SiC Austempered 2h at 300 °C

Source: Author

The As Sintered samples presents a fine dispersion of carbides into ferrite but its morphology is different. Samples with 2 wt% SiC presents fine carbides and highly stabilized ferrite zones next to graphite nodules due SiC dissociation and Si dissolution. On the other hand samples with 3 wt% SiC have a larger area of stabilized ferrite with fine carbides precipitated in grain boundaries due carbon rejection of stabilized ferrite, it still maintain darker areas of ferrite with dispersed carbides inside the ferrite grains. The martempered samples exhibits a tempered martensite structure with areas were the microstructure turns into bainite, this is more noticeable by looking the microstructure of the austempered samples which presents ferrite laths growing from austenitic grains. Figure 36 presents a comparison at 10.000X between the microstructures of Fe + 0.6C + 4Ni + 1Mo + 3SiC alloy under As Sintered and martempered and tempered conditions. Figure 37 compares the morphology of the microstructure of Fe + 0.6C + 4Ni + 1Mo and Fe + 0.6C + 4Ni + 1Mo + 3SiC austempered samples.

Fig. 36 - SEM images of Fe + 0.6C + 4Ni + 1Mo + 3SiC in the As Sintered and the martempered and tempered condition

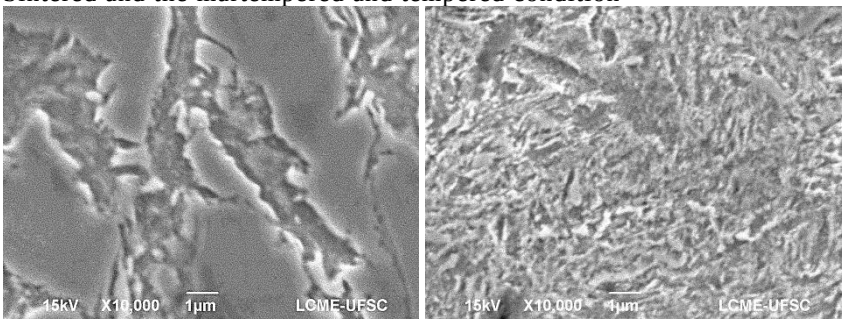

Fe + 0.6C + 4Ni + 1Mo + 3SiC as sintered

Fe + 0.6C + 4Ni + 1Mo + 3SiC martempered 1h and tempered 2h at 530 °C

Source: Author

The microstructural difference between As Sintered and heat treated samples becomes clear in the micrographs above. The As Sintered samples has carbides precipitated in the ferrite grain boundaries while the martempered and tempered samples shows a much finer and acicular microstructure proper of tempered martensite.

Fig. 37 - SEM images of Fe + 0.6C + 4Ni + 1Mo and Fe + 0.6C + 4Ni + 1Mo + 3SiC + 3SiC in the austempered condition

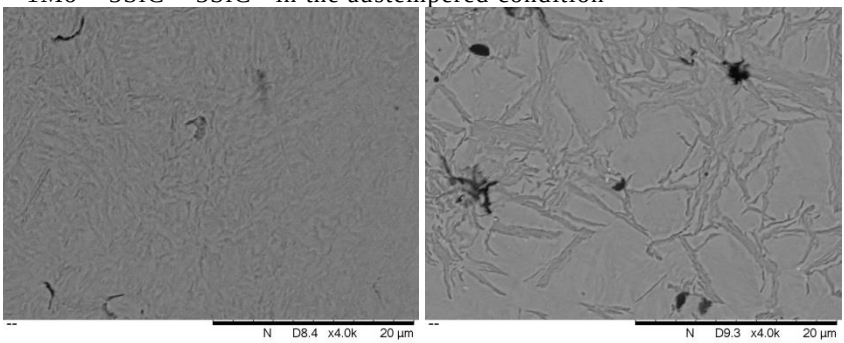

Fe + 0.6C + 4Ni + 1Mo Austempered 2h at 300°C

Fe + 0.6C + 4Ni + 1Mo + 3SiC Austempered 2h at 300°C

Source: Author

Base austempered alloy shows fine ferrite laths growing into retained austenite while the samples with SiC additions shows larger and but fewer bainitic ferrite laths, this change of morphology explains why the mechanical resistance of the austempered alloys drops with the

SiC content and the strain hardening exponent rises. Larger ferrite grains into bainite allows more dislocation movement within the grains, lowering it hardness and yield strength but allowing more plastic strain and strain hardening.

Graphite nodule presence was also measured using SEM and EDS scanning. Figure 38 shows the elements intensity peaks along a graphite module.

Fig. 38 - Elements x-ray intensity peaks along a graphite nodule of a Fe + 0.6C + 4Ni + 1Mo + 3SiC As Sintered sample

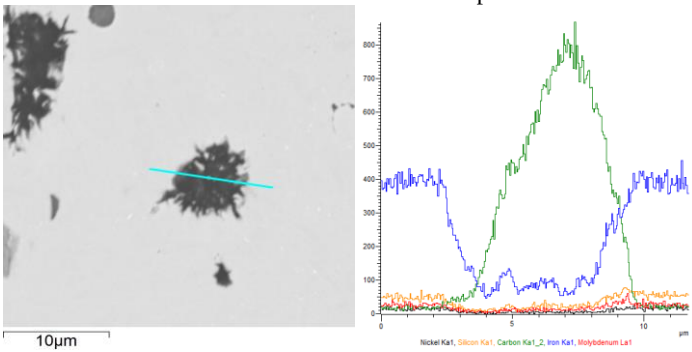

Source: Author

Graphite nodules also influences the hardness distribution of these materials, graphite nodules surrounded by a ferrite ring have a lower hardness while its surroundings became hardened for solid solution and hardenability increase effect of Si into the alloy. Figure 38 shows a $HV_{0.01}$ microhardness profile. Figure 40 shows a SEM image and a EDS of an indentation done over a graphite nodule in a Fe + 0.6C + 4Ni + 1Mo + 3SiC alloy martempered and tempered at 530 °C.

Fig. 39 - Microhardness profile of Fe + 0.6C + 4Ni + 1Mo and Fe + 0.6C + 4Ni + 1Mo + 3SiC martempered and tempered 2h at 530°C

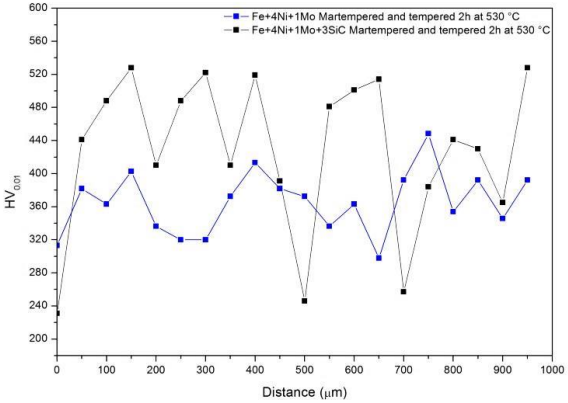

Source: Author

Fig. 40 - SEM image and EDS scan on a vickers microindentation done over a graphite nodule , measured hardness was of $HV_{0.01}$ 133

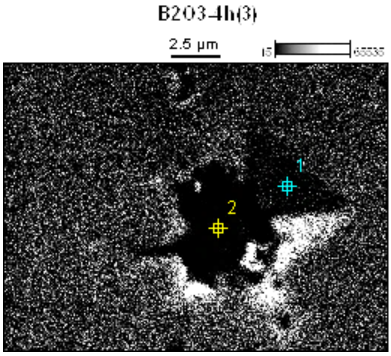

	C-K	*O-K*	*Si-K*	*Fe-K*	*Ni-K*	*Mo-L*
B2O3-4h(3)_pt1	14.70		1.51	80.50	2.75	0.54
B2O3-4h(3)_pt2	95.33	0.00	0.15	4.23	0.14	0.15

Source: Author

As shown by figs. 39 and 40 the presence of graphite nodules and segregated Si causes microstructural and mechanical heterogeneity, these factors must be considered of interest when analyzing the wear behavior of these alloys.

6. CONCLUSIONS

Sintered self-lubricating steels were produced by powder injection molding and plasma assisted debinding and sintering. These were heat treated and its mechanical properties and microstructural evolution were studied. From these studies was found that:

- Nickel segregation occurred during the sintering process. This caused the apparition of harder zones into the microstructure probably constituted by martensite and retained austenite.

- SiC addition to the base alloy decreases the severity in terms of volumetric changes of the transformation $\gamma \leftrightarrow \alpha + Fe_3C$.

- Si dissolution into the matrix rises the A_1 temperature due to ferrite stabilization.

- Si dissolution into the matrix modifies the microstructure of the specimens, not only by generating highly stabilized ferrite zones around graphite nodules as found in previous works but also by modifying the morphology of the matrix's microstructure after heat treatment.

- SiC addition improves mechanical resistance for all the samples with a peak at 2% SiC. This trend is reversed for austempered samples as its bainitic microstructure appears to be coarser than the one found in the samples without SiC.

- SiC addition improves ductility of the samples and favors strain hardening in samples that weren't martempered.

7. SUGGESTIONS FOR FUTURE RESEARCH

For continuity of the current work the following subjects for research are suggested:

- To further study the strain hardening behavior of these alloys under different modes of deformation.
- To study the influence of the degree of disorder and defects presents in the graphite nodules in the tribological behavior of these materials.
- To study the tribological behavior of the heat treated samples
- A more detailed study on the microstructural influence of Si under several heat treatment conditions (temperatures and time).
- To study the mechanical properties and microstructure of these alloys using different ceramic powders as precursor phases.
- To develop new matrix alloys and heat treatments for these steels with enhanced mechanical and tribological properties.

REFERENCES

ASM INTERNATIONAL HANDBOOK COMMITEE. Heat Treating. In: ASM INTERNATIONAL (Ed.). . **ASM Handbook**. Cleveland: The Materials Information Company, 1991. v. IVp. 15–28.

ASM INTERNATIONAL HANDBOOK COMMITEE. Powder Metal Technologies and Applications. In: ASM INTERNATIONAL (Ed.). . **ASM Handbook**. The Materials Information Company, 1998. p. 2762.

ASTM INTERNATIONAL. **Standard Test Method for Tensile Strain-Hardening Exponents (n-Values) of Metallic Sheet Materials**, 2007.

BEDOLLA-JACUINDE, A. et al. Sliding wear behavior of austempered ductile iron microalloyed with boron. **Wear**, p. 1–9, 2015.

BHADESHIA, H. K. D. H. Lower Bainite Transformation and the Significance of Carbide Precipitation. **Acta Metallurgica**, v. 28, p. 1103–1114, 1980.

BHADESHIA, H. K. D. H. Upper & Lower Bainite. In: **Bainite in Steels**. Institute of Materials, Minerals and Mining, 2001a. p. 189–200.

BHADESHIA, H. K. D. H. Mechanical Properties. In: **Bainite in Steels**. Institute of Materials, Minerals and Mining, 2001b. p. 285–342.

BINDER, C. **DESENVOLVIMENTO DE NOVOS TIPOS DE AÇOS SINTERIZADOS AUTOLUBRIFICANTES A SECO COM ELEVADA RESISTÊNCIA MECÂNICA ALIADA A BAIXO COEFICIENTE DE ATRITO VÍA MOLDAGEM DE PÓS POR INJECÃO**. Universidade Federal de Santa Catarina, 2009.

BINDER, C. et al. “Fine tuned” steels point the way to a focused future. **Metal Powder Report**, v. 65, n. 4, p. 29–37, maio 2010.

BRIS CABRERA, J. L. **Comportamiento Mecánico de Aceros Sinterizados de Alta Densidad**. UNIVERSITAT POLITÉCNICA DE CATALUNYA, 2006.

BUCH, A.; GOLDSCHMIDT, S. Influence or Porosily on Elaslic

Moduli of Sinlered Malerials. **Materials Science and Engineering**, v. 5, n. 2, 1969.

CAI, M. et al. Effects of Si on Microstructural Evolution and Mechanical Properties of Hot-rolled Ferrite and Bainite Dual-phase Steels. **ISIJ International**, v. 51, n. 3, p. 476–481, 2011.

CLAUSS, F. J. **Solid Lubricants and Self-Lubricating Solids**. I ed. New York: Academic Press Inc., 1972.

CUI, G. et al. The bronze–silver self-lubricating composite under sea water condition. **Tribology International**, v. 60, p. 83–92, abr. 2013.

DE MELLO, J. D. B. et al. Effect of the metallic matrix on the sliding wear of plasma assisted debinded and sintered MIM self-lubricating steel. **Wear**, v. 301, n. 1-2, p. 648–655, abr. 2013.

DENG, X. et al. Deposition and tribological behaviors of ternary BCN coatings at elevated temperatures. **Surface and Coatings Technology**, p. 1–5, out. 2014.

DRESSELHAUS, M. S. Future directions in carbon science. **Annu. Rev. Mater. Sci.**, v. 27, p. 1–34, 28 mar. 1997.

DU, G. Y. et al. Research on Frictional Behavior of Tungsten Disulfide Thin Films Prepared by Rf Magnetron Sputtering on Restless Steel. **Physics Procedia**, v. 32, p. 532–538, jan. 2012.

DUBRUJEAUD, B.; VARDAVOULIAS, M.; JEANDIN, M. The role of porosity in the dry sliding wear of a sintered ferrous alloy. **Wear**, v. 174, n. 1-2, p. 155–161, 1994.

FERNÁNDEZ CASTAÑÓN, J. **INFLUENCIA DE LA POROSIDAD COMPORTAMIENTO EN SERVICIO DE ACEROS SINTERIZADOS : ANÁLISIS TEÓRICO Y EXPERIMENTAL**. Universidad de Oviedo, 2014.

FURLAN, K. P. et al. Thermal Stability of the MoS2 Phase in Injection Moulded 17-4 PH Stainless Steel. **Journal of Materials Research and Technology**, v. 1, n. 3, p. 134–140, out. 2012.

GERMAN, R. M. **Powder Metallurgy & Particulate Materials Processing**. Princeton: Metal Powder Industries Federation, 2005.

HARRY, C. **Heat Treater's Guide: Practices and Procedures for Irons and Steels - Heat Treating Processes and Related Technology Introduction**. ASM International, 1995.

HERTELÉ, S.; DE WAELE, W.; DENYS, R. A generic stress-strain model for metallic materials with two-stage strain hardening behaviour. **International Journal of Non-Linear Mechanics**, v. 46, n. 3, p. 519–531, 2011.

KATO, H. et al. Wear and mechanical properties of sintered copper–tin composites containing graphite or molybdenum disulfide. **Wear**, v. 255, n. 1-6, p. 573–578, ago. 2003.

KIM, J.-H. et al. Strain rate dependent tensile behavior of advanced high strength steels: Experiment and constitutive modeling. **Materials Science and Engineering: A**, v. 559, p. 222–231, 2013.

KOVÁČIK, J. et al. Effect of composition on friction coefficient of Cu–graphite composites. **Wear**, v. 265, n. 3-4, p. 417–421, jul. 2008.

MIYOSHI, K. **Solid Lubrication Fundamentals and Applications**. 1st. ed. Cleveland: CRC Press, 2001.

MOUSTAFA, S. . et al. Friction and wear of copper–graphite composites made with Cu-coated and uncoated graphite powders. **Wear**, v. 253, n. 7-8, p. 699–710, out. 2002.

ÖZMEN, Y.; TANAKA, A.; SUMIYA, T. Effect of humidity on the tribological behavior of diamond-like carbon (DLC) film coated on WC-Co by physical vapor deposition method. **Surface and Coatings Technology**, v. 133-134, p. 455–459, 2000.

REBELO, D. **MORFOLOGIA E ESTRUTURA DOS NÓDULOS DE GRAFITE GERADOS PELA DISSOCIAÇÃO DE SiC NA SINTERIZAÇÃO DE LIGAS FERROSAS**. Universidade Federal de Santa Catarina, 2014.

ROHATGI, P. K.; RAY, S.; LIU, Y. Tribological properties of metal matrix-graphite particle composites. **International Materials Reviews**, v. 37, n. 1, p. 129–152, 1992.

SCHROEDER, R. et al. Internal lubricant as an alternative to coating steels. **Metal Powder Report**, v. 65, n. 7, p. 24–31, nov. 2010.

STACHOWIAK, G. W.; BATCHELOR, A. W. SOLID LUBRICATION AND SURFACE TREATMENTS. In: **Engineering Tribology**. Third Edit ed. p. 419–459.
STRAFFELINI, G. et al. Dry rolling-sliding wear of austempered cast iron. **Wear**, v. 271, n. 9-10, p. 1602–1608, 2011.

WELZ, S. **Identification of carbon allotropes in carbide derived carbon using electron microscopy**. University of Illinois, Chicago, 2003.

ZHANG, D.; SHEN, B.; SUN, F. Study on tribological behavior and cutting performance of CVD diamond and DLC films on Co-cemented tungsten carbide substrates. **Applied Surface Science**, v. 256, n. 8, p. 2479–2489, fev. 2010.

ZHANG, J.; DING, H.; MISRA, R. D. K. Enhanced strain hardening and microstructural characterization in a low carbon quenching and partitioning steel with partial austenization. **Materials Science and Engineering: A**, v. 636, p. 53–59, 2015.

ZHANG, Z. et al. Theoretical Calculation of the Strain-Hardening Exponent and the Strength Coefficient of Metallic Materials. **Journal of Materials Engineering and Performance**, v. 15, n. 1, p. 19–22, 2006.

ZOUARI, M. et al. A comparative investigation of the tribological behavior and scratch response of polyester powder coatings filled with different solid lubricants. **Progress in Organic Coatings**, v. 77, n. 9, p. 1408–1417, set. 2014.